The toxicity of antiprion antibodies is mediated by the flexible tail of the prion protein

Sonati, Tiziana ; Reimann, Regina R ; Falsig, Jeppe ; Baral, Pravas Kumar ; O'Connor, Tracy ; Hornemann, Simone ; Yaganoglu, Sine ; Li, Bei ; Herrmann, Uli S ; Wieland, Barbara ; Swayampakula, Mridula ; Rahman, Muhammad Hafizur ; Das, Dipankar ; Kav, Nat ; Riek, Roland ; Liberski, Pawel P ; James, Michael N G ; Aguzzi, Adriano

Abstract: Prion infections cause lethal neurodegeneration. This process requires the cellular prion protein (PrP(C); ref. 1), which contains a globular domain hinged to a long amino-proximal flexible tail. Here we describe rapid neurotoxicity in mice and cerebellar organotypic cultured slices exposed to ligands targeting the 1 and 3 helices of the PrP(C) globular domain. Ligands included seven distinct monoclonal antibodies, monovalent Fab1 fragments and recombinant single-chain variable fragment miniantibodies. Similar to prion infections, the toxicity of globular domain ligands required neuronal PrP(C), was exacerbated by PrP(C) overexpression, was associated with calpain activation and was antagonized by calpain inhibitors. Neurodegeneration was accompanied by a burst of reactive oxygen species, and was suppressed by antioxidants. Furthermore, genetic ablation of the superoxide-producing enzyme NOX2 (also known as CYBB) protected mice from globular domain ligand toxicity. We also found that neurotoxicity was prevented by deletions of the octapeptide repeats within the flexible tail. These deletions did not appreciably compromise globular domain antibody binding, suggesting that the flexible tail is required to transmit toxic signals that originate from the globular domain and trigger oxidative stress and calpain activation. Supporting this view, various octapeptide ligands were not only innocuous to both cerebellar organotypic cultured slices and mice, but also prevented the toxicity of globular domain ligands while not interfering with their binding. We conclude that PrP(C) consists of two functionally distinct modules, with the globular domain and the flexible tail exerting regulatory and executive functions, respectively. Octapeptide ligands also prolonged the life of mice expressing the toxic PrP(C) mutant, PrP(Δ94-134), indicating that the flexible tail mediates toxicity in two distinct PrP(C)-related conditions. Flexible tail-mediated toxicity may conceivably play a role in further prion pathologies, such as familial Creutzfeldt-Jakob disease in humans bearing supernumerary octapeptides.

DOI: https://doi.org/10.1038/nature12402

Aguzzi, Adriano (2013). The toxicity of antiprion antibodies is mediated by the flexible tail of the prion protein. Nature, 501(7465):102-106.
DOI: https://doi.org/10.1038/nature12402

The flexible tail of the prion protein mediates the toxicity of antiprion antibodies

Tiziana Sonati[1,*], Regina R. Reimann[1,*], Jeppe Falsig[1,*], Pravas Kumar Baral[2], Tracy O'Connor[1], Simone Hornemann[1], Sine Yaganoglu[1], Bei Li[1], Uli S. Herrmann[1], Barbara Wieland[2], Mridula Swayampakula[2], Muhammad Hafizur Rahman[3], Dipankar Das[3], Nat Kav[3], Roland Riek[4], Pawel P. Liberski[5], Michael N. G. James[2], and Adriano Aguzzi[1†]

[1] Institute of Neuropathology, University Hospital Zurich, Switzerland

[2] Department of Biochemistry, University of Alberta, Canada

[3] Department of Agricultural, Food and Nutritional Science, University of Alberta, Canada

[4]ETH Zurich, Physical Chemistry, ETH Honggerberg, 8093 Zurich, Switzerland

[5]Laboratory of Electron Microscopy and Neuropathology, Department of Molecular Pathology and Neuropathology, Medical University of Lodz, Lodz, Poland.

[*] These authors contributed equally to this work

[†]Corresponding author:

Adriano Aguzzi

Institute of Neuropathology, University Hospital of Zurich

Schmelzbergstrasse 12, CH-8091 Zurich, Switzerland

Tel: +41-44-255-2108, Email address: adriano.aguzzi@usz.ch

Prion infections cause lethal neurodegeneration. This process requires the cellular prion protein[1] PrP^C which contains a globular domain (GD) hinged to a long N-proximal flexible tail (FT)[2]. Here we describe rapid neurotoxicity in mice and cerebellar organotypic cultured slices (COCS) exposed to ligands targeting the α1 and α3 helices of the GD. Ligands included seven distinct monoclonal antibodies[3], monovalent $F(ab)_1$ fragments, and recombinant single-chain miniantibodies derived therefrom. Similarly to prion infections[4-6], toxicity of GD ligands required neuronal PrP^C, was exacerbated by PrP^C overexpression, was associated with calpain activation, and was antagonized by calpain inhibitors. Neurodegeneration was accompanied by a burst of reactive oxygen species, and was suppressed by antioxidants. Furthermore, genetic ablation of the superoxide-producing enzyme NOX2 protected mice from GD ligands. We also found that neurotoxicity was prevented by deletions of the octapeptide repeats within the FT. These deletions did not appreciably compromise GD antibody binding, suggesting that the FT is required to transmit toxic signals that emanate from the GD and trigger oxidative stress and calpain activation. Supporting this view, various octapeptide ligands were not only innocuous to both COCS and mice, but also prevented the toxicity of GD ligands while not interfering with their binding. We conclude that PrP^C consists of two functionally distinct modules, with the GD and the FT exerting regulatory and executive functions, respectively. Octapeptide ligands also prolonged the life of mice expressing the toxic PrP^C mutant[7], $PrP_{\Delta 94\text{-}134}$, indicating that the FT mediates toxicity in two distinct PrP^C-related conditions. FT-mediated toxicity may conceivably play a role in further prion pathologies, such as familial Creutzfeldt-Jakob disease in humans bearing supernumerary octapeptides.

The infectious prion PrP^{Sc}, which causes transmissible spongiform encephalopathies, is a pathological conformer of PrP^{C}, a glycosylphosphatidyl-inositol (GPI) linked cell-surface protein encoded by the *Prnp* locus[8]. Only PrP^{C}-expressing cells are damaged by prion infections[1], suggesting that neurotoxicity is triggered by PrP^{C}-PrP^{Sc} interactions on cell membranes. In an effort to model such interactions, we exposed cerebellar organotypic cultured slices (COCS)[4,9] to a panel of anti-PrP antibodies directed against well-defined PrP^{C} epitopes[3]. Supplementary Figure 1 summarizes our main findings, and Supplementary Table 1 lists all abbreviations.

PrP^{C}-overexpressing COCS (derived from *tga20* mice that are hypersensitive to prion diseases[5]) were treated with 5 antibodies against the flexible tail of PrP^{C} (FT, residues 23-123) (ref. 10) and with 12 antibodies against the globular domain of PrP^{C} (GD, residues 124-230; Supplementary Table 2; Fig. 1a). Seven of the antibodies targeting the GD induced dramatic loss of cerebellar granule cells (CGC) at 67 nM and one was toxic at 333 nM, whereas four were innocuous (Fig. 1b). None of three high-affinity antibodies to the octapeptide repeats (OR, residues 50-90 embedded within the FT) were neurotoxic (Fig. 1b). Antibodies POM3 and D13, which bind the "charged cluster-2"[11] (CC2, residues 95-110), were innocuous at 67 nM but neurotoxic at 200 nM (Fig. 1b). None of the tested antibodies were toxic to $Prnp^{o/o}$ COCS (Supplementary Fig. 2a). The identity of the targeted epitopes appeared to be a better predictor of PrP^{C} antibody toxicity than their affinity to PrP^{C}, suggesting that neurotoxicity resulted from the interaction of antibodies with specific PrP^{C} domains (Supplementary Table 2).

The mechanisms of neurotoxicity were further explored using POM1, a highly toxic antibody targeting the GD. Wild-type (*wt*) and *tga20* COCS lost most granule cells (CGC) within 28 and 14 days post-exposure (dpe) to POM1, respectively (Fig. 2a-c). Controls included POM1-treated $Prnp^{o/o}$ COCS[12], *tga20* COCS treated with pooled mouse immunoglobulins (IgG), and

tga20 COCS treated with POM1 preincubated with full length recombinant mouse PrP ($rmPrP_{23-230}$). All of these controls were unaffected (Fig. 2d), indicating that POM1 toxicity was PrP^C-dependent. Propidium iodide (PI) staining, a marker of cell death, revealed that CGC membrane integrity was compromised before overt neuronal loss in POM1-treated *tga20* COCS. The prevalence of PI^+ cells peaked at 3-5 days and decreased thereafter, suggesting removal of dead cells (Fig. 2e, Supplementary Fig. 3). Therefore POM1-mediated neurotoxicity was dependent on *Prnp* gene-dosage as well as duration and dosage of the antibody treatment. Similarly to neurotoxicity in prion infections[6], neuronal PrP^C expression was necessary and sufficient for POM1 toxicity (Supplementary Fig. 4a-c), suggesting that its effects were cell-autonomous to neurons. Finally, treatment of COCS with an anti-NOGO receptor antibody was innocuous, indicating that toxicity was not a generic consequence of binding to GPI-linked receptors (Supplementary Fig. 4d).

It was previously reported that antibody-mediated crosslinking of PrP^C at the cell surface leads to neurotoxicity[11]. However, both monovalent and divalent POM1, POM17 and POM19 derivatives ($F(ab)_1$ fragments, $F(ab)_2$ fragments, and recombinant single-chain (scFv) miniantibodies) induced neurotoxicity in *tga20* COCS but not in $Prnp^{o/o}$ COCS (Fig. 2f-g and Supplementary Figs. 5 and 2b). Hence neurotoxicity was rapidly induced by structurally diverse GD ligands, and did not require antibody effector functions mediated by Fc receptors (Fig. 2f-g) or complement (Supplementary Fig. 6).

Neurotoxicity may result from conformational changes imposed onto PrP^C by POM1. We therefore solved the crystal structure of the protein complex containing POM1 $F(ab)_1$ bound to recombinant mouse PrP (residues 120-230, $rmPrP_{120-230}$; Supplementary Fig. 7; Supplementary Tables 2 and 3). The POM1 epitope on $rmPrP_{120-230}$ was discontinuous and included the C-

terminal part of the β1-α1 loop, the N-terminal part of helix α1, as well as a segment of helix α3. The surface area of the interface was ca. 580 $Å^2$, and involved primarily the POM1 heavy chain (Supplementary Movie 1 and Supplementary Fig. 7). Comparisons with published structures[2,10,13,14] indicate that $F(ab)_1$POM1 binding did not cause conformational distortions in the GD. We also studied the binding interface of $scFv^{POM1}$ complexed with full-length recombinant mouse PrP (residues 23-230, $rmPrP_{23-230}$) by solution nuclear magnetic resonance (NMR) spectroscopy. Overlays of the NMR spectra of $rmPrP_{23-230}$ with those of the $scFv^{POM1}$:$rmPrP_{23-230}$ complex did not reveal appreciable perturbations of the FT (Supplementary Fig. 8), whereas PrP^C residues in contact with $scFv^{POM1}$ in the GD displayed chemical shift changes as expected from the crystal structure. Moreover, we found subtle perturbations in the chemical shifts in the β1/β2 regions that were not present in the crystal structure (Supplementary Fig. 8).

To investigate whether the FT contributes to the neurotoxicity of GD ligands, we administered POM1 to COCS expressing either $PrP_{\Delta 32-93}$ (lacking most of the FT) or $PrP_{\Delta 94-110}$ (lacking the CC2)[15,16] (Supplementary 9a). Whilst $PrP_{\Delta 94-110}$ COCS experienced POM1-dependent neurodegeneration, COCS overexpressing $PrP_{\Delta 32-93}$ were resistant to all tested neurotoxic antibodies, POM1, POM4, POM8, and POM19 (Fig. 3a, Supplementary Figs. 4b and 9b,c). The affinities of POM1 $F(ab)_1$ fragments for N-terminally truncated prion protein (PrP_{90-230}) and full-length recombinant PrP_{23-230} were similar (2.9 and 2.5 nM, respectively; Supplementary Table 2), confirming that the resistance of $PrP_{\Delta 32-93}$ COCS to POM1 effect was not due to any steric changes compromising the POM1 binding site.

These results suggested that the FT is required for GD ligands-mediated toxicity. If so, engaging FT with antibodies might prevent the toxicity of GD antibodies. Indeed, preincubation

of *tg*a*20* COCS with OR antibodies (POM2 or POM11), or with scFv derivatives thereof, blocked POM1 toxicity (Fig. 3b-c). Interestingly, low concentrations of POM3 and D13 also blocked POM1 toxicity, although these antibodies were intrinsically toxic at higher concentrations (Fig. 3b). Hence CC2 binders acted similarly to pharmacological "partial antagonists", triggering opposite effects depending on the presence or absence of additional ligands. Crucially, neither POM2 nor POM3 sterically hinder POM1 binding[3,4] and the non-toxic GD antibody POM5, which did not compete for the POM1 epitope[3] (Supplementary Fig. 9d) did not rescue neurotoxicity (Supplementary Fig. 9e). We conclude that the domain executing toxicity resides within the FT.

Although we suspected that POM1 treatment would result in apoptosis, electron micrographs of POM1-treated COCS revealed cell death with morphology distinct from typical apoptosis (Supplementary Fig. 10). Furthermore, POM1 did not induce caspase activity (Fig. 3e), and the caspase antagonist zVAD conferred no neuroprotection against POM1 (Fig. 3d). Instead, proteolysis of the calpain substrates, α-fodrin[17] and calpain activity was significantly raised after $scFv^{POM1}$ and POM1 treatment (Fig. 3e, f), and calpain inhibition prevented POM1-mediated toxicity (Fig. 3d). None of the compounds used in the above experiments affected the viability of IgG-treated COCS (Supplementary Fig. 11a). Hence POM1 neurotoxicity results in calpain-dependent cell death, similarly to prion-infected COCS[4].

Oxidative stress is a common promoter of neurodegeneration[18], raising the question of its possible involvement in the toxicity of GD ligands. Indeed, the reactive oxygen species (ROS) scavengers, ascorbate (0.1-2.5 mM) and N-acetyl cysteine, conferred neuroprotection against POM1-mediated toxicity (Fig. 3d, Supplementary Fig. 11b, c). Long-term incubation of POM1 with ascorbate did not reduce the binding of POM1 to $rmPrP_{23-230}$, ruling out that antioxidants

affected antibody stability (Supplementary Fig. 11c). The cell-impermeable isoascorbate was also protective, suggesting that the relevant ROS were extracellular (Fig. 3d, Supplementary 11a). Moreover, inhibition of nitric oxide production showed no protective effect, whereas the superoxide dismutase mimetic MnTBAP abolished POM1 neurotoxicity (Fig. 3d and Supplementary Fig. 11a), pointing to superoxide rather than nitric oxide as the critical ROS species. NADPH oxidases (NOX) are an important source of extracellular superoxide[19], and indeed $scFv^{POM1}$ treatment induced a superoxide spike in COCS that was suppressed by the NADPH oxidase (NOX) inhibitor, diphenyleneiodonium chloride (DPI; Fig. 3g). Hence GD ligands initiate a cascade of events which ultimately triggers the activation of NADPH oxidases.

We then investigated the effects of GD ligands in intact mice. POM1 or IgG were stereotactically injected into the cerebella of *tga20* and $Prnp^{o/o}$ mice (Fig. 4a, Supplementary Fig. 12a). Sequential manganese-enhanced magnetic resonance imaging (MEMRI)[20] revealed hypointense lesions indicative of edema formation arising at 4-72h post-injection. At their peak, such lesions occupied up to 2.5% and 20% of the total cerebellar volume of *wt* and *tga20* mice, respectively (Fig. 4a, b and Supplementary Fig. 12b). Histology revealed CGC chromatin condensation beginning at 5h post-injection (Supplementary Fig. 13a), conspicuous tissue edema by 24h (Supplementary Fig. 13b), and pyknotic CGC death with limited perifocal hemorrhages by 72h (Fig. 4a). After one week, we found substantial neuronal loss and glial scars (Supplementary Fig. 13c). No such changes were observed in IgG-treated *tga20* or POM1-treated $Prnp^{o/o}$ mice (Fig. 4a, b, and Supplementary Fig. 13). Hypointense lesions also arose after stereotactic injection of POM1 or D13 into *tga20* hippocampi, histologically identified as sites of extensive degeneration of CA3 and dentate gyrus neurons (Supplementary Fig. 14). Intracerebellar injection of $scFv^{POM1}$ also induced extensive lesions in *tga20* cerebella and smaller

lesions in *wt* cerebella (Fig. 4c). Lesions did not arise when scFv^{POM1} was pre-incubated with rmPrP$_{23-230}$, and when scFv^{POM1} was administered to *Prnp*$^{o/o}$ mice (Fig. 4c). ScFv^{POM2} was innocuous to *tga20* mice (Fig. 4c). Hence these *in vivo* results confirm that toxicity was dependent on GD binding and on PrP^{C} expression levels, but neither on antigen crosslinking nor on any antibody effector functions. As with COCS, neuron-restricted PrP^{C} expression sufficed to confer scFv^{POM1} susceptibility *in vivo* (Fig. 4d), whereas mice expressing PrP$_{\Delta 32-93}$[15] were resistant to scFv^{POM1} toxicity despite higher PrP$_{\Delta 32-93}$ expression, PrP$_{\Delta 94-110}$ mice[16] lacking only the CC2 domain of PrP^{C} experienced toxicity (Fig. 4e and Supplementary Figs. 4b and 9c).

Mice expressing PrP$_{\Delta 94-134}$, which lacks the central domain of PrP^{C}, develop spontaneous neurodegeneration whose pathogenesis is poorly understood[7] (Supplementary Fig. 9a). If this pathology were mediated by the FT, it might be alleviated by anti-FT antibodies. Indeed, a single intraventricular injection of POM2 to newborn (P0) PrP$_{\Delta 94-134}$ mice resulted in significantly increased median survival (26 *vs*. 22 days, *n*=9; Fig. 4f), suggesting that the FT is also involved in the neurotoxicity of these PrP^{C} mutants.

To determine whether ROS were involved in POM1 neurotoxicity *in vivo*, we administered the enterically activated antioxidant, acetylated hydroxytyrosol[21] (AcHyt) to *tga20* mice. Five of six untreated, but only one of six AcHyt-treated, *tga20* mice developed cerebellar lesions upon scFv^{POM1} injection (Fig. 4g; Supplementary Fig. 15). POM1-treated NADPH oxidase 2 (NOX2) deficient mice[22] displayed much smaller lesions than POM1-treated *wt* controls (Fig. 4h), implicating NOX2 as the crucial source of ROS in this model.

The data reported above uncover a critical role for the FT as the effector domain of PrP^{C}-mediated neuronal death. FT-mediated toxicity appears to arise from inappropriate gain of deleterious functions, rather than loss of homeostatic interactions, because shortening or steric

masking of the FT conferred protection from neurotoxicity (Supplementary Fig. 1a-b), and because most *Prnp* transgenes bearing interstitial FT deletions[5,15,23] are innocuous. Similar mechanisms may be operative in mice[24] and humans[25-27] expressing PrP^{C} variants with supernumerary OR (Supplementary Fig. 1c). These syndromes are surprising since the OR lie outside the PrP^{Sc} amyloid core and are dispensable for prion generation[15,23]. If the disease caused by supernumerary OR is mechanistically equivalent to that elicited by GD ligands, agents effective against GD ligand toxicity may also be beneficial to patients with OR insertions.

Might the toxicity of GD ligands also emulate the docking of PrP^{Sc} to PrP^{C}? This conjecture is supported by the role of activated calpains, which are involved in prion infections. Perhaps PrP^{Sc} oligomers engage PrP^{C} through its α1/α3 helices similarly to the GD ligands (Supplementary Fig. 1c). In this scenario soluble PrP^{C} may reduce prion toxicity[28] by intercepting oligomers and preventing them from interacting with membrane-bound PrP^{C}. Furthermore, the dramatic effects of GD ligands in *vivo* suggest that anti-GD autoimmunity may cause neurological conditions, and that it may be worthwhile screening patients with idiopathic neurodegeneration for such autoantibodies.

Methods summary

Slices were prepared using a vibratome from 10-12 old-days pups according to a previously published protocol[9]. Viability was assessed by quantifying propidium iodide incorporation or NeuN immunoreactive area using analysis software analySIS vs5.0. $F(ab)_1$ and $F(ab)_2$ fragments were generated by ficin digestion, isolated after protein A elution and further purified by size exclusion chromatography. Single chain fragments of POM1 and POM2 were expressed in Escherichia Coli (periplasm) and purified by Ni-NTA agarose columns. Recombinant mouse

prion proteins (23-230 and 90-230) were generated in bacteria and purified as reported[29,30]. The POM1 epitope was determined by X-ray and NMR analyses as described in the Supplementary Methods section. Antibodies and respective fragments were stereotactically injected into mouse brains; lesions were visualized by MEMRI and quantified with Para Vision software (Version 5. Opl3, Bruker). SPR experiments were performed with a BIAcore X100 instrument and interpreted with BIAcore T100 Evaluation Software, version 2.0.3.

A detailed description of methods and materials is given in the Supplementary Information section.

References

1 Brandner, S. *et al.* Normal host prion protein necessary for scrapie-induced neurotoxicity. *Nature* **379**, 339-343, (1996).

2 Riek, R. *et al.* NMR structure of the mouse prion protein domain PrP(121-231). *Nature* **382**, 180–182, (1996).

3 Polymenidou, M. *et al.* The POM monoclonals: a comprehensive set of antibodies to non-overlapping prion protein epitopes. *PLoS ONE* **3**, e3872, (2008).

4 Falsig, J. *et al.* Prion pathogenesis is faithfully reproduced in cerebellar organotypic slice cultures. *PLoS Pathog* **8**, e1002985, (2012).

5 Fischer, M. *et al.* Prion protein (PrP) with amino-proximal deletions restoring susceptibility of PrP knockout mice to scrapie. *EMBO J* **15**, 1255-1264, (1996).

6 Mallucci, G. *et al.* Depleting neuronal PrP in prion infection prevents disease and reverses spongiosis. *Science* **302**, 871-874, (2003).

7 Baumann, F. *et al.* Lethal recessive myelin toxicity of prion protein lacking its central domain. *Embo J* **26**, 538-547, (2007).

8 Aguzzi, A. & Calella, A. M. Prions: protein aggregation and infectious diseases. *Physiol Rev* **89**, 1105-1152, (2009).

9 Falsig, J. & Aguzzi, A. The prion organotypic slice culture assay - POSCA. *Nat Protoc.* **3**, 555-562, (2008).

10 Riek, R., Hornemann, S., Wider, G., Glockshuber, R. & Wüthrich, K. NMR characterization of the full-length recombinant murine prion protein, mPrP(23-231). *FEBS Lett* **413**, 282-288, (1997).

11 Solforosi, L. *et al.* Cross-linking cellular prion protein triggers neuronal apoptosis in vivo. *Science* **303**, 1514-1516, (2004).

12 Büeler, H. R. *et al.* Normal development and behaviour of mice lacking the neuronal cell-surface PrP protein. *Nature* **356**, 577-582, (1992).
13 Zahn, R. *et al.* NMR solution structure of the human prion protein. *Proc Natl Acad Sci U S A* **97**, 145–150, (2000).
14 Wuthrich, K. & Riek, R. Three-dimensional structures of prion proteins. *Adv Protein Chem* **57**, 55-82, (2001).
15 Flechsig, E. *et al.* Prion protein devoid of the octapeptide repeat region restores susceptibility to scrapie in PrP knockout mice. *Neuron* **27**, 399-408, (2000).
16 Bremer, J. *et al.* Axonal prion protein is required for peripheral myelin maintenance. *Nat Neurosci* **13**, 310-318, (2010).
17 Wang, K. K. Calpain and caspase: can you tell the difference? *Trends Neurosci* **23**, 20-26, (2000).
18 Fatokun, A. A., Stone, T. W. & Smith, R. A. Oxidative stress in neurodegeneration and available means of protection. *Front Biosci* **13**, 3288-3311, (2008).
19 Sorce, S. & Krause, K. H. NOX enzymes in the central nervous system: from signaling to disease. *Antioxid Redox Signal.* **11**, 2481-2504, (2009).
20 Silva, A. C., Lee, J. H., Aoki, I. & Koretsky, A. P. Manganese-enhanced magnetic resonance imaging (MEMRI): methodological and practical considerations. *NMR Biomed* **17**, 532-543, (2004).
21 Granados-Principal, S., Quiles, J. L., Ramirez-Tortosa, C. L., Sanchez-Rovira, P. & Ramirez-Tortosa, M. C. Hydroxytyrosol: from laboratory investigations to future clinical trials. *Nutr Rev.* **68**, 191-206, (2010).
22 Pollock, J. D. *et al.* Mouse model of X-linked chronic granulomatous disease, an inherited defect in phagocyte superoxide production. *Nat Genet* **9**, 202-209, (1995).
23 Yamaguchi, Y. *et al.* Biological and biochemical characterization of mice expressing prion protein devoid of the octapeptide repeat region after infection with prions. *PLoS ONE* **7**, e43540, (2012).
24 Chiesa, R., Piccardo, P., Ghetti, B. & Harris, D. A. Neurological illness in transgenic mice expressing a prion protein with an insertional mutation. *Neuron* **21**, 1339-1351, (1998).
25 Krasemann, S. *et al.* Prion disease associated with a novel nine octapeptide repeat insertion in the PRNP gene. *Brain Res Mol Brain Res* **34**, 173-176, (1995).
26 Mead, S. *et al.* Inherited prion disease with six octapeptide repeat insertional mutation--molecular analysis of phenotypic heterogeneity. *Brain* **129**, 2297-2317, (2006).
27 Vital, C., Gray, F., Vital, A., Ferrer, X. & Julien, J. Prion disease with octapeptide repeat insertion. *Clin Exp Pathol* **47**, 153-159, (1999).
28 Meier, P. *et al.* Soluble dimeric prion protein binds PrP(Sc) in vivo and antagonizes prion disease. *Cell* **113**, 49-60, (2003).
29 Zahn, R., von Schroetter, C. & Wüthrich, K. Human prion proteins expressed in Escherichia coli and purified by high- affinity column refolding. *FEBS Lett* **417**, 400–404, (1997).
30 Lysek, D. A. & Wuthrich, K. Prion protein interaction with the C-terminal SH3 domain of Grb2 studied using NMR and optical spectroscopy. *Biochemistry* **43**, 10393-10399, (2004).

Acknowledgements

We thank Shozo Izui, Hannah Monyer, Dennis Burton, and Giovanna Mallucci for reagents and mice, Stefan Schauer and the Functional Genomics Center Zurich for advice and help with affinity determinations, Andreas Steingötter, Udo Ungethüm, Magdalini Polymenidou, Agnes Lau and Annika Keller for input, Rita Moos, Beata Sikorska, Cinzia Tiberi, Petra Schwarz, Ahmet Varol, Karina Arroyo and Mirzet Delic for technical help. AA is the recipient of an Advanced Grant of the European Research Council and is supported by grants from the European Union (PRIORITY, LUPAS), the Swiss National Foundation, the Foundation Alliance BioSecure and the Novartis Research Foundation. JF is supported by the Swiss Center of Transgenic Expertise and by a career development award of the University of Zürich. Research support from PrioNet Canada and Alberta Prion Research Institute (APRI) for the work conducted in the Canadian laboratories is gratefully acknowledged. PPL and AA are supported by Polish Swiss Research grant nr PSPB-062/2010. This paper is dedicated to the memory of Dr. Marek Fischer, who created the *tga20* mouse line.

Author contributions

TS, JF and AA conceived the study. Planning and execution were performed by TS with significant contributions from RRR, JF and additional contribution from TO, SH, SY, BL and UH. MEMRI was established and performed by RRR, EM was performed by PL, scFv were cloned and produced by BW, MS, MHR, DD and NK, X-ray crystallography was performed by PKB and MNGJ, and NMR experiments were performed by SH with additional contributions from RR. TS, JF and AA wrote the manuscript.

Authors information:

X-ray crystallographic coordinates and structure factor files have been deposited in the RSCB PDB database under the accession number 4H88. Reprints and permissions information is available at www.nature.com/reprints. The authors declare no competing financial interests. Correspondence and request for reagents should be addressed to AA (Adriano. Aguzzi@usz.ch).

Figure legends

Figure 1. Epitope specificity of the neurotoxicity mediated by antiprion antibodies. a, Antibody binding sites on $rmPrP_{23-230}$. POM6-9, 13, 15 and 17 bind helix α1 and compete with POM1[3]. POM6 and POM7 (light orange) show additional binding sites at helix α2 (dark orange), whereas POM5 recognizes a unique epitope at the β2-α2 transition (green, Supplementary Table 2). GD image was rendered using the PDB structure 2L1H. **b**, NeuN morphometry of *tga20* COCS treated with various antibodies to FT and GD epitopes (same color codes as in panel a). Treatment modalities: 67 nM, 10 days (&); 200 nM, 21 days (#); 333 nM, 14 days ($), or 67 nM, 21 days (unlabeled columns). CGC loss was induced by antibodies to helices α1 (light violet, orange, red) and α3 (blue). Antibodies binding the CC2 (magenta) were toxic only at higher concentrations and after protracted incubation. Antibodies against the OR (turquoise) were consistently innocuous. Ordinate: percentage of $NeuN^+$ pixels within the CGC layer, normalized against treatment with pooled IgG. One-way ANOVA with Dunnett's post-test, ***P<0.001, **P<0.01, mean ± s.d, n=9 biological replicates.

Figure 2. Antibody-mediated toxicity in cerebellar slices does not require crosslinking or antibody effector functions. a, *Tga20* COCS were treated with POM1 (67 nM) or with pooled IgG (67nM, used here and in all following figures as negative control) for 14 dpe, cut transversally as indicated in the left panel, and stained with hematoxylin and eosin. POM1 treatment caused COCS thinning and CGC ablation. Arrows: Purkinje cells. **b,** *Tga20* COCS were exposed to POM1 or to control pooled IgG (67 nM, 10 dpe), immunostained for the neuronal marker NeuN, and imaged by confocal laser scanning microscopy. POM1 (lower panels) induced loss of NeuN immunoreactivity. **c**, Concentration and time-dependent CGC loss

in POM1-exposed *tga20* (left panel; 14 dpe) and *wt* COCS (right panel; antibody concentration: 270 nM). One-way-ANOVA with Dunnett's post-test. **d**, Preincubation of POM1 with rmPrP$_{23\text{-}230}$ (molar ratio 1:60) suppressed neurodegeneration of *tga20* COCS (antibody treatment: 67 nM, 14 dpe). One-way-ANOVA with Tukey's post-test. **e**, COCS were treated with POM1 (67 nM) and scored for NeuN^{+} (blue) and PI^{+} (red) area coverage within the CGL. PI incorporation peaked at 3 dpe, coinciding with the maximum slope of NeuN decay. **f**, *Prnp*$^{o/o}$ and *tga20* COCS were incubated with POM1 holoantibody, divalent F(ab)$_2$, monovalent F(ab)$_1$, or scFv derivatives of POM1. NeuN morphometry identified severe neurodegeneration after exposure (10 dpe) to each ligand irrespectively of its valence. Red dashed lines (here and henceforth) delineate independent experiments normalized against their respective IgG control assays. One-way-ANOVA with Dunnett's post-test. **g**, Treatment of *tga20* COCS for 21 days with F(ab)$_1$ fragments of POM17 and 19 (134 nM) resulted in similar toxicity as with holoantibodies, whereas F(ab)$_1$POM5 and F(ab)$_1$POM15 were innocuous. One-way-ANOVA with Tukey's post-test. For all experiments, data in bar charts are presented as mean ± s.d, n=9 biological replicates; ***P<0.001.

Figure 3. Neuroprotection against GD ligand toxicity. a, NeuN morphometry of COCS treated with POM1 antibody (167 nM, 28 dpe). *Wt* and PrP$_{\Delta 94\text{-}110}$ COCS (line L46), but neither PrP$_{\Delta 32\text{-}93}$ nor *Prnp*$^{o/o}$ COCS, experienced POM1 toxicity. One-way-ANOVA with Tukey's post-test. **b**, *Tga20* COCS were pre-treated with various antibodies directed against the FT (37°C, 30 min) and exposed to POM1 (yellow bars: 67 nM, 14 dpe). POM2, POM11, POM3 and D13 (67 nM) prevented POM1 toxicity. White bars: omission of POM1. One-way-ANOVA with Dunnett's post-test**. c**, Pre-treatment with scFv^{POM2} (264 nM) protected *tga20* COCS from scFv^{POM1} (264

nM; 10 dpe). One-way-ANOVA with Dunnett's post-test**. d**, Effect of various compounds (listed in Supplementary Table 4) on POM1 toxicity (67 nM). Compound concentrations are reported in Supplementary Information. Yellow: no pre-treatment. Red: protective compounds. White: non-protective compounds. Grey: IgG control-treated slices. POM1 neurotoxicity was blocked by antioxidants and calpain inhibitors, but not by caspase or iNOS inhibitors. Isoascorbate, a cell impermeable analogue of ascorbate, was also protective. One-way-ANOVA with Dunnett's post-test**. e,** Cultures (3 dpe) were assayed for DEVDase (black) and LLYase activity (red), indicative of caspase and calpain activity, respectively. Protease activity was normalized to protein amount ± s.d. One-way-ANOVA with Dunnett's post-test, mean ± s.d., *n*=3 pools of 18 slices. Whilst staurosporine (24h) increased both activities, POM1 treatment increased LLYase but not DEVDase activity. **f,** Immunodetection of α-fodrin in *tga20* COCS (3 dpe). $ScFv^{POM1}$ treatment increased total α-fodrin cleavage and the calpain-specific fragment of 145 kDa (*n*= 3 pools of 6 slices; mean ± s.d. underneath blot; two-tailed student t-test, *P*=0.0054). **g,** $ScFv^{POM1}$-treated COCS (400 nM, 24h) were harvested and analyzed for ROS production by lucigenin assay in the presence or absence of DPI. One-way-ANOVA with Dunnett's post-test, mean ± s.d., *n*=4, each datapoint represents a pool of 9 slices). For all experiments, data in bar charts are presented as mean ± s.d, *n*=9 biological replicates; ***$P<0.001$, **$P<0.01$.

Figure 4. Anti-PrP antibody toxicity in vivo. a, MEMRI scans showed hypointense lesions in POM1-treated (6 μg in 2 μl) *wt* and *tga20* mice (left panels) 72 hours post intracerebellar injection (pii). Yellow dashed lines delineate the lesions. Histology (middle and right panels) revealed CGC destruction (stars) and edema. Rectangles: region magnified in the corresponding rightmost panel. *Tga20* Purkinje cells (arrow), which do not express PrP^C, were largely preserved.

b, Lesion volumes at 4, 24, and 72h pii as percentages of total cerebellar volumes in *wt, tg*a*20*, and $Prnp^{o/o}$. Grey: control injections (6 µg, mean ± s.d., *n*=4 except for $Prnp^{o/o}$ at 72h *n*=3, *tg*a*20* at 4h and 24h *n*=6, one-way-ANOVA with Dunnett's post-test). **c**, Lesions occurred in *tg*a*20* (*n*=4) and *wt* (*n*=4) mice after injection of $scFv^{POM1}$ (2 µg) but not after $scFv^{POM2}$ (*n*=4), or $scFv^{POM1}$ (2 µg) preincubated with recombinant $mPrP_{23-230}$ (molar ratio 1:5, 24h, *n*=4). $ScFv^{POM1}$-treatment was innocuous to $Prnp^{o/o}$ (*n*=3) mice (mean ± s.d., two-tailed student t-test). **d**, MEMRI volumetry (24h pii) of NSE-PrP (*n*=4) and $Prnp^{o/o}$ (*n*=7) mice injected with $scFv^{POM1}$ (3 µg; mean ± s.d., two-tailed student t-test). **e**, MEMRI volumetry 24h pii of $scFv^{POM1}$ into $PrP_{\Delta 94-110}$(L52, *n*=3), $PrP_{\Delta 32-93}$ (*n*=5), and *wt* (*n*=8) (mean ± s.d.; two-tailed Student t-test). **f**, Survival of mice expressing a $PrP_{\Delta 94-134}$ transgene was prolonged by intraventricular POM2 (*n*=9) treatment *vs.* IgG control (*n*=5) (4 µg, Mantel-Cox-test). **g**, *Tg*a*20* mice 24h pii of $scFv^{POM1}$ (2 µg) pre-treated with acetylated hydroxytyrosol, (mean ± s.d., *n*=6, one-tailed student t-test. *P*= 0.013). **h**, MEMRI volumetry at 24h pii of $scFv^{POM1}$ (3 µg) into $Prnp^{o/o}$ (*n*=7), *wt* (*n*=5) and NOX2-deficient (*n*=11) mice (mean ± s.d., one-tailed student t-test).

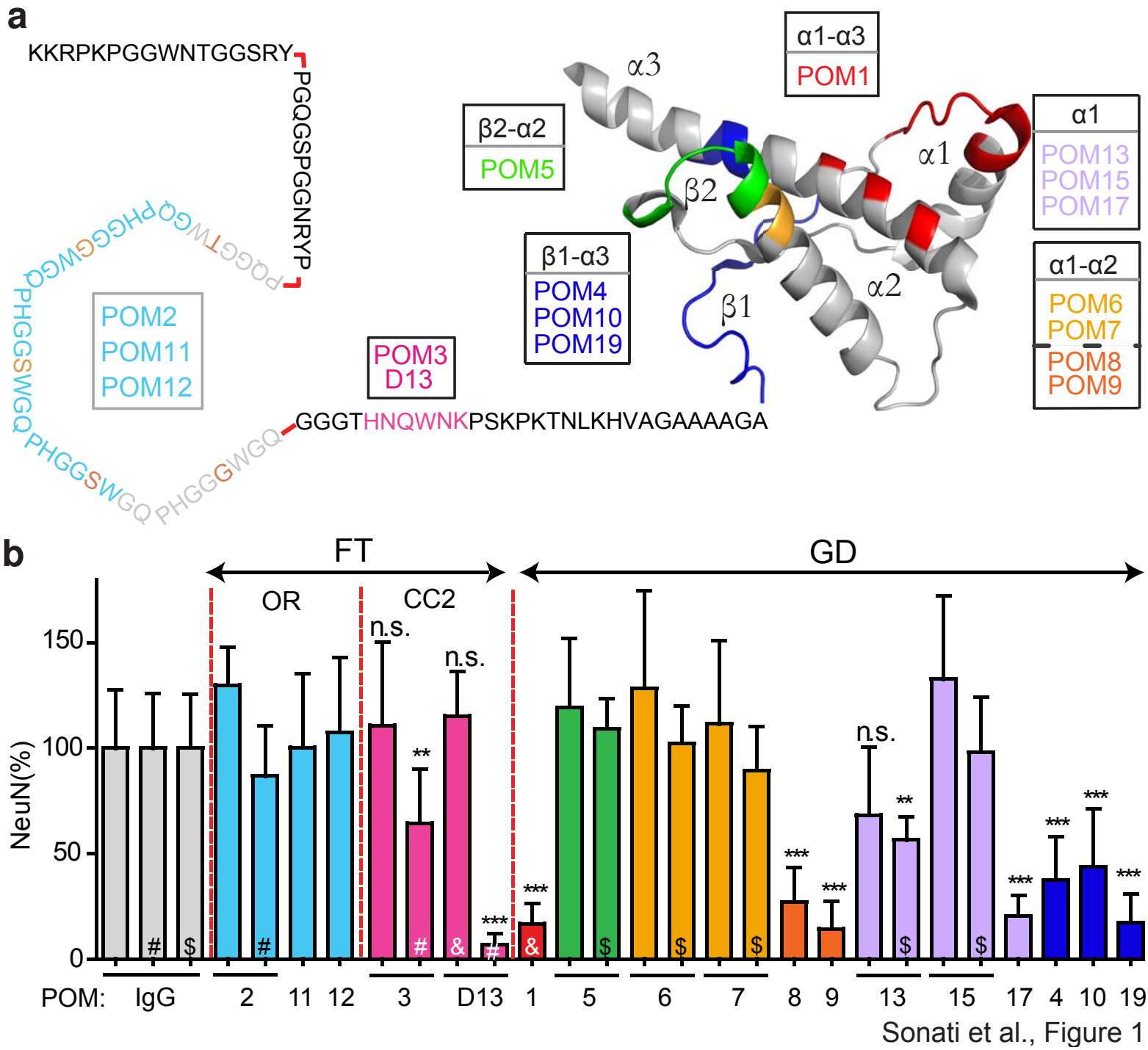
a
KKRPKPGGWNTGGSRY
PGQGSPGGNRYP
PQGGTWGQPHGGGWGQ
PHGGSWGQ PHGGSWGQ PHGGGWGQ
POM2
POM11
POM12
POM3
D13
GGGTHNQWNKPSKPKTNLKHVAGAAAAGA
α1-α3
POM1
α3
β2-α2
POM5
β2
α1
α1
POM13
POM15
POM17
β1-α3
POM4
POM10
POM19
α2
β1
α1-α2
POM6
POM7
POM8
POM9
b
FT
GD
OR
CC2
n.s.
n.s.
n.s.
NeuN(%)
150
100
50
0
POM: IgG 2 11 12 3 D13 1 5 6 7 8 9 13 15 17 4 10 19
Sonati et al., Figure 1

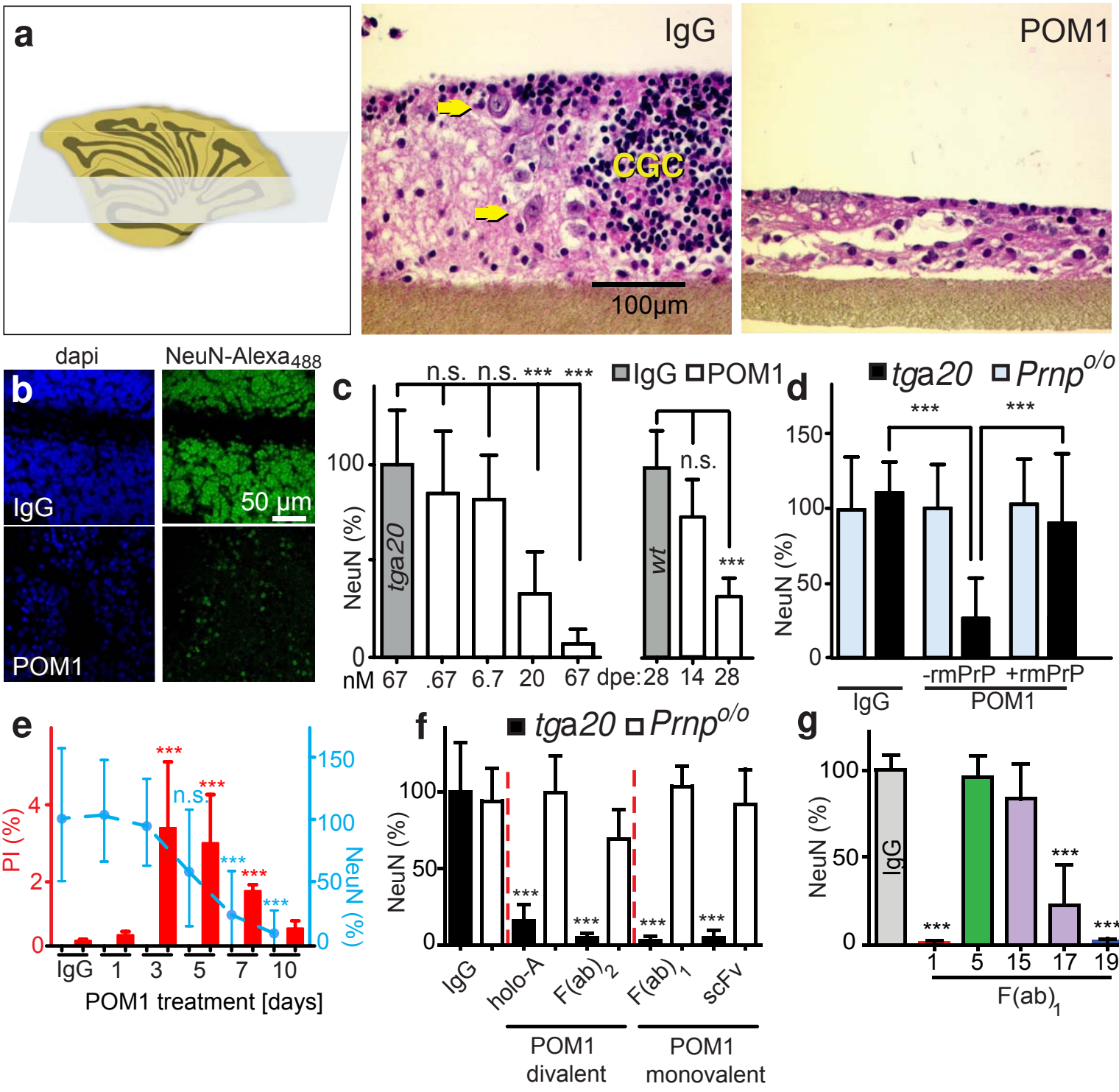

Sonati et al., Figure 2

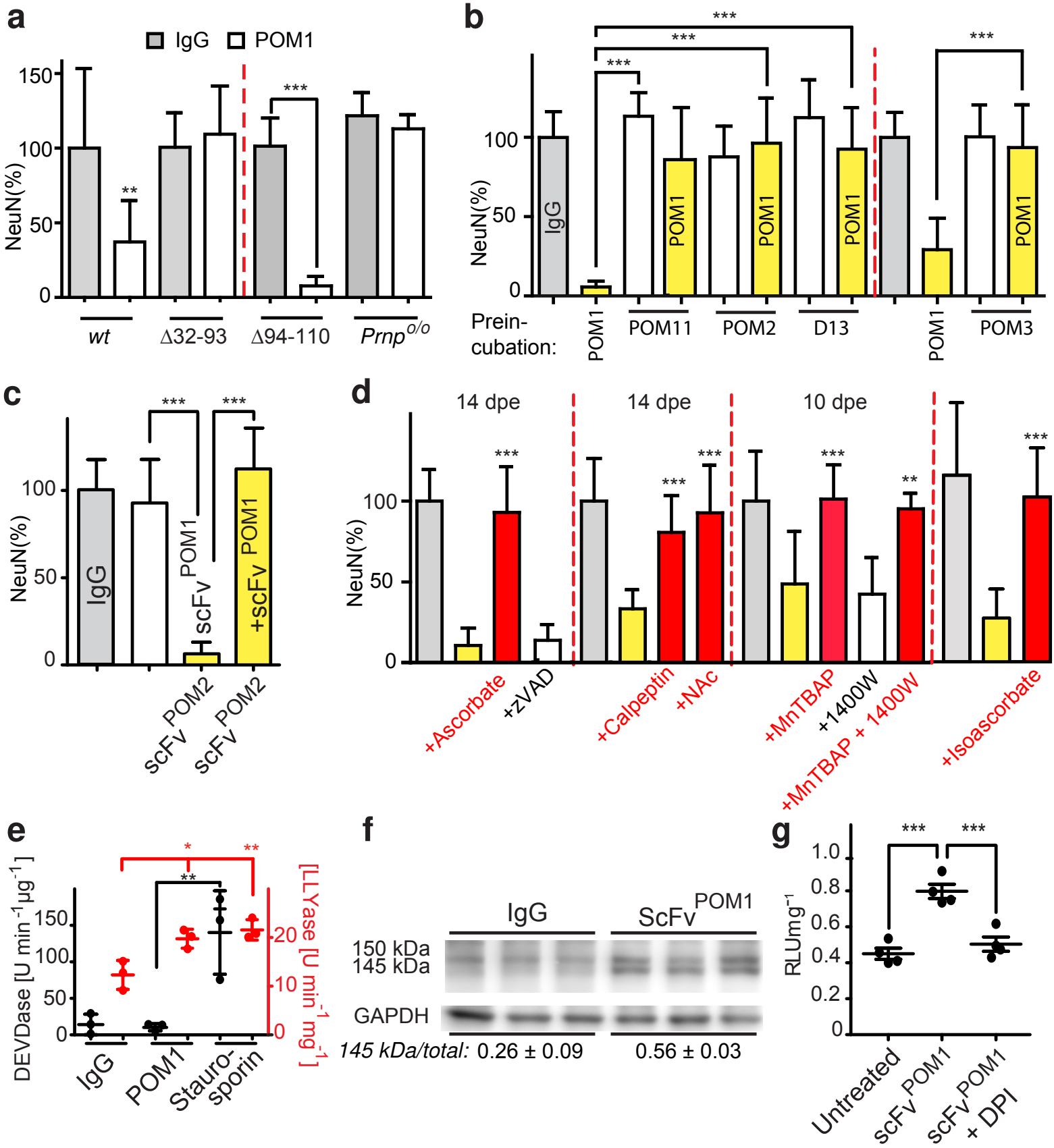

Sonati et al., Figure 3

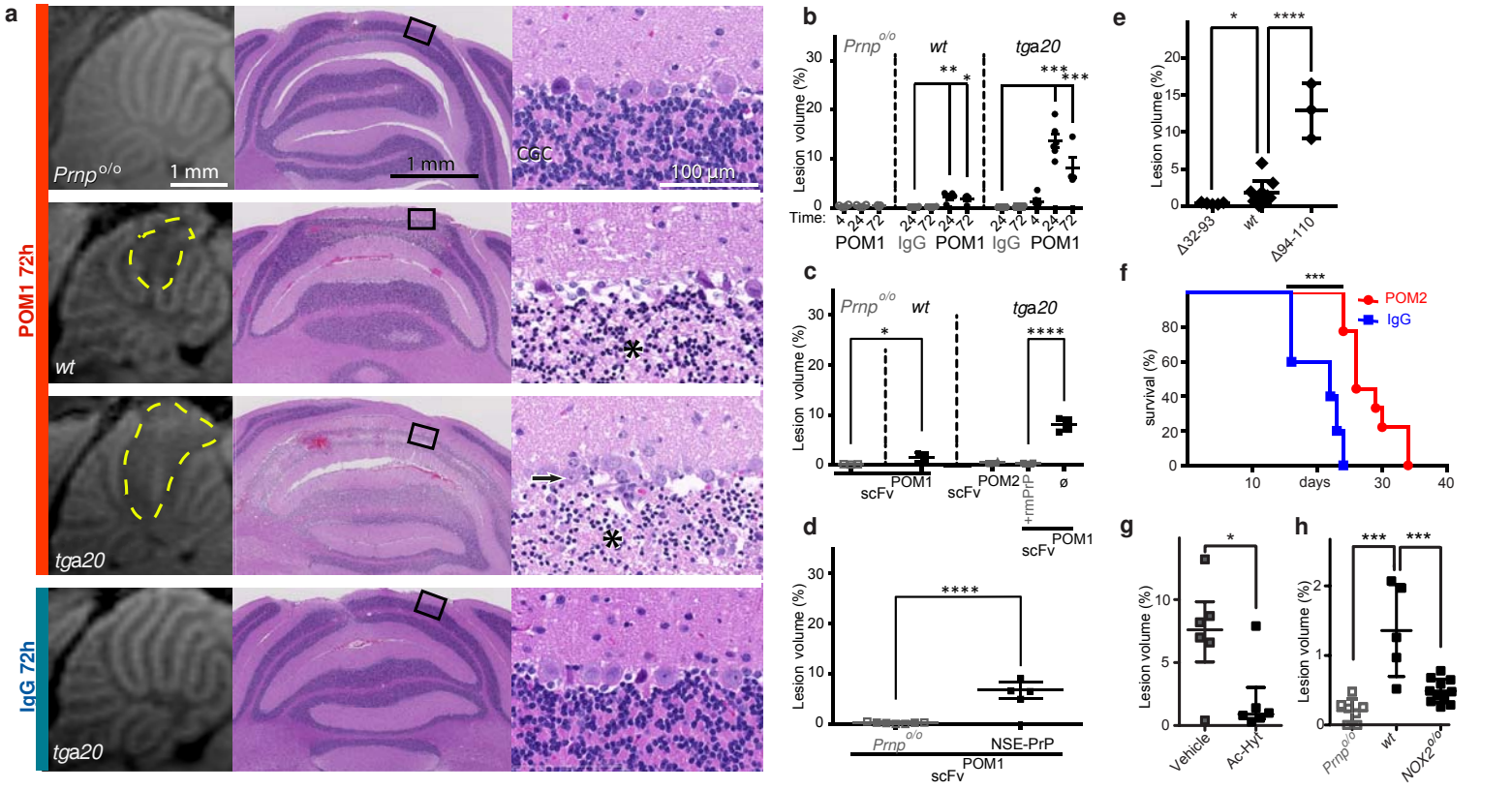

Sonati et al., Figure 4

Supplementary Materials and Methods

Chemicals and mice

All compounds were purchased from Sigma/Aldrich unless otherwise stated. GABA-Aα6-CRE mice were generated on a C57BL/6xCBA background and back-crossed to a *Prnp*$^{o/o}$ background[12,31]. Tg37 mice allowing for conditional PrP deletion were generated on a *Prnp*$^{o/o}$ FVB background[32]. GABA-$A_{\alpha 6}$-CRE^{-};loxPrP-tg37 littermates were used as negative controls (PrP^{CGC+}). B6.129S6-*Cybb*^{tm1Din}/J (NOX2)-deficient mice were generated on a mixed C57BL/6xSv129 background and backcrossed to C57BL/6[22]. *Prnp*$^{o/o}$, *Prnp*$^{o/o}$;*tga20*$^{+/+}$ (*tga20*), *Prnp*$^{o/o}$;*C4/C4* (PrP$_{\Delta 32\text{-}93}$), *Prnp*$^{o/o}$;*1046* (PrP$_{\Delta 94\text{-}134}$)[7], *Prnp*$^{o/o}$;*L46* (PrP$_{\Delta 94\text{-}110}$)[16], *Prnp*$^{o/o}$;*L52* (PrP$_{\Delta 94\text{-}110}$), *Prnp*$^{o/o}$;NSE-PrP$^{+/+}$ (*NSE-PrP*) and *Prnp*$^{o/o}$;MBP-PrP$^{+/+}$ (*MBP-PrP*) mice were on a mixed 129Sv/BL6 background, and *wt* mice on a C57BL/6 background[5,12,15,16,33,34]. *Prnp*$^{o/o}$;*L52* (PrP$_{\Delta 94\text{-}110}$) was previously reported[16]. CD11b-HSVTK mice[35] on a C57BL/6 background were crossed to *Prnp*$^{o/o}$;*tga20*$^{+/+}$. All offspring were *Prnp*$^{+/o}$;*tga20*$^{+}$ and CD11b-HSVTK positive offspring were referred to as *tga20*$^{TK+}$. All mouse experiments were performed on 6-9 month old males and females, conformed to Swiss law, and were approved by the Animal Experimentation Committee of the Canton of Zurich (permits 200/2007 and 130/2008).

Animal surgery

Mice were anesthetized with isoflurane and placed in a motorized stereotaxic frame controlled by software with a 3D brain map, allowing for real-time monitoring of needle placement (Neurostar). The skull was exposed by cutting along the midline and a small hole was drilled using a surgical drill and the needle mounted in an electronic micro-injector unit was placed for cerebellar injection at the following lambda coordinates: AP -2.3mm, ML 0mm, DV 2mm and for

hippocampal injection at the following bregma coordinates: AP -2mm, ML 1.7mm, DV 2.2mm, angle in ML/DV plane 15°. Antibodies (2 µl) were injected at a flow-rate of 0.5 µl min^{-1} and the needle was left in place for 1 min. Mice were sutured and received an injection of buprenorphinum (0.1 µg g^{-1} bodyweight).

Hydroxytyrosol treatment

Mice were treated with acetylated hydroxytyrosol starting 7 days prior to injection with 2g l^{-1} in drinking water.

Newborn injections

Newborn mice (P0) were injected with a thin Hamilton syringe into the lateral ventricle (2 µL of 2 mg ml^{-1} IgG or POM2 solution into each hemisphere) according to previously reported protocols[36].

Manganese-Enhanced Magnetic Resonance Imaging (MEMRI)

Mice received five intraperitoneal injections of $MnCl_2$ (40 mg kg^{-1}, 20 mM in H_2O and bicine, pH 7.4) at 12h intervals[37]. The last injection was administered immediately after the stereotaxic injection. Mice were imaged under isoflurane anesthesia at 4h, 24h and 72h post-surgery in a 4.7-Tesla small-animal MRI system (Bruker Pharmascan). Mice were placed in a bed equipped with a mouse whole-body radio frequency transmitter coil and a mouse head surface-coil receiver (Bruker Pharmascan). Body temperature was maintained with a warming blanket. T-1 weighted brain images were obtained using a 3D gradient-echo sequence (TR: 15 ms, TE: 2.5 ms, FA: 20 deg, Average:10, Matrix: 265/265/126, Field of View: 2x2.56x2 cm^3, acquisition time: 1h, voxel size: 78x100x156 μm^3)[38].

Quantification was performed with ParaVision software (Version 5. Opl3, Bruker). Cerebellar lesions were quantified by two region of interests (ROIs) corresponding to the lesioned and total cerebellar area were set for each optical slice of the 3D dataset. For hippocampal lesion quantification, the volume of non-affected CA3 was measured. ROIs were set on the ipsilateral and contralateral side of injection. Volumes for each ROI were calculated by multiplying the sum of the ROI area times the voxel height. Data are presented as the lesion volume divided by the total cerebellar volume, i.e. lesion volume (%) or as CA3 volume (mm^3), separated by ipsilateral versus contralateral side.

Organotypic brain culture preparation

Organotypic cerebellar slice cultures, 350 µm thick, were prepared from 10-11 day-old pups according to a previously published protocol[9]. Free-floating sections were cut in Gey's balanced salt solution (GBSS) (NaCl 8 g l^{-1}, KCl 0.37 g l^{-1}, Na_2HPO_4 0.12 g l^{-1}, $CaCl_2$ $2H_2O$ 0.22 g l^{-1}, KH_2PO_4 0.09 g l^{-1}, $MgSO_4$ $7H_2O$ 0.07 g l^{-1}, $MgCl_2$ $6H_2O$ 0.210 g l^{-1}, $NaHCO_3$ 0.227 g l^{-1}) supplemented with the glutamate receptor antagonist kynurenic acid (1 mM) (GBSSK) at 4°C. Slices were placed on a 6-well Millicell-CM Biopore PTFE membrane insert (Millipore). Residual buffer was removed and the inserts were transferred to a cell culture plate and cultured in "slice-culture medium" (50% vol/vol MEM, 25% vol/vol basal medium Eagle and 25% vol/vol horse serum supplemented with 0.65% glucose (w/vol), penicillin/streptomycin and glutamax (Invitrogen)). Cultures were kept in a standard cell incubator (37°C, 5% CO_2, 95% humidity) and the culture medium was exchanged three times per week.

Antibody treatment was randomly assigned to individual wells and initiated after a 10-14 day recovery period allowing the initial gliosis induced by tissue preparation to subside. Slices were harvested for biochemical analyses or fixed for immunocytochemical analysis at various time

points. For microglia depletion experiments, *tga20*$^{TK+}$ slices were treated with ganciclovir (GCV, 5 µg ml^{-1}) for 14 days prior to antibody treatment. At this time point less than 1% of microglia were left in the tissue[39].

Pharmacological treatment of COCS

Drug treatment was initiated at the time of antibody addition and drugs were re-added at every medium change. Appropriate drug concentrations were determined by literature search, assuming that slice culture uptake of compounds were similar to other cell culture systems. The toxicity of each compound was tested in parallel on IgG and POM1 slices; if toxicity occurred, drugs were retested at a lower concentration. Drug and concentration used were ascorbate (1.5 mM), isoascorbate (1.5mM), MnTBAP (100 µM), benzyloxycarbonyl-Val-Ala-Asp (OMe) fluoromethylketone (zVAD-fmk, 40 µM), diphenyleneiodonium chloride (DPI, 5 µM), N-([3-(Aminomethyl)phenyl]methyl)- ethanimidamide dihydrochloride (1400W, 20 µM), N-benzyloxycarbonyl-L-leucylnorleucinal (calpeptin, 20 µM), N-acetylcystein (NaC, 1 mM).

Protein analysis

COCS were washed twice in PBS. Cerebellar tissue was then scraped off the membrane using 10 µl per slice of PBS with 0.5% DOC, 0.5% NP-40 supplemented with PMSF (1 µM) and complete mini protease inhibitor cocktail (Roche), and homogenized by trituration using a 30G syringe. Protein concentration was determined using the bicinchoninic acid assay (Pierce). Samples were prepared in loading buffer (NuPAGE, Invitrogen) and boiled at 95°C for 5 min. Proteins (10 µg per lane) were separated on a 12% Bis-Tris polyacrylamide gel or for higher molecular weight proteins on a 4-12% gradient gel (NuPAGE, Invitrogen) and blotted onto a nitrocellulose membrane. Membranes were blocked with 5% w/vol Topblock (Fluka) in Tris-buffered saline

supplemented with Tween (150 mM NaCl, 10 mM Tris HCl, 0.05% Tween 20 (vol/vol)) and incubated with primary antibodies in 1% Topblock. Primary mouse monoclonal antibodies used were: POM1, POM2, mouse IgG_1 antibody raised against PrP^C (anti-PrP^C; 200 ng ml^{-1}), mouse anti-α-fodrin (AA6, 100 ng ml^{-1}, Millipore) and anti-GAPDH (200 ng ml^{-1}, Millipore). Secondary antibodies were horseradish peroxidase (HRP)-conjugated rabbit anti–mouse IgG_1 (1:10,000, Zymed), goat anti–rabbit IgG_1 (1:10,000, Zymed), and rabbit anti–goat IgG_1 (1:10,000, Zymed). Blots were developed using SuperSignal West Pico chemiluminescent substrate (Pierce) and visualized using the VersaDoc system (model 3000, Bio-Rad). PNGase treatment was performed using a commercially available kit, according to the manufacturer's protocol (New England Biolabs). In brief, 10 µg protein was treated with 2 µl denaturation buffer in a 20 µl reaction and incubated for 15 min at 95°C. A reaction mixture of 2.6 µl G7, 2.6 µl NP-40 (10%), as well as 0.5 µl PNGase was added and samples were incubated for 2h at 37°C. Samples were then mixed with loading dye, cooked and analyzed by western blotting. Cerebella from 10 day-old pups were homogenized (10% w/v) in 0.32 M sucrose in 1x PBS supplemented with 4-(2-Aminoethyl)-Benzene sulfonyl fluoride HCL (AEBSF, 1 mM) and complete mini protease inhibitor cocktail (Roche) using a tissue Ribolyser (Qiagen). PrP^C expression in the brains of PrP deletion mutants was analyzed by PrP-specific sandwich ELISA[3]. Briefly, samples were incubated in POM1-coated ELISA plates (overnight at 4°C). Plates were then washed and incubated with biotinylated POM19 (1.6 ng ml^{-1}) for 1h at 37°C. Avidin-HRP (1:1000) (BD-Pharmigen) was used as detection antibody (1h, 37°C). After 3 washes, stabilized chromogen (Invitrogen) was added, incubated for 30 minutes at 37°C, and absorbance was read at 450 nm. All samples were analyzed at dilutions falling within the logarithmic range of the calibration curve ($rmPrP_{23-230}$: 0.62-80 ng ml^{-1}).

Generation of POM monoclonals, F(ab)$_1$POM1 and F(ab)$_2$POM1 fragments

POM monoclonal antibodies were generated as published[3]. F(ab)$_1$POM1 and F(ab)$_2$POM1 fragments were generated by ficin digestion and purified on a protein A column according to manufacturer's protocol (Pierce). Protein A flow-through containing F(ab)$_1$POM1 was collected, concentrated by Amicon ultra-15 centrifugal units (Millipore). F(ab)$_1$POM1 was further purified by size exclusion chromatography (Superdex75 10/300 GL, GE Healthcare) using PBS and a flow rate of 0.5 ml min^{-1}. Pure fractions were pooled, concentrated and stored at -20°C. The concentrations of the IgG and F(ab)$_1$POM fragments were determined by measuring their absorbance at 280 nm in a UV-VIS photometer using an extinction coefficient (E) 0.1% at 280 nm of 1.35. Aldolase (158 kDa), conalbumin (75 kDa) and ovalbumin (43 kDa) were used as control molecular weight markers. The purity of the fragments was checked by Coomassie-stained SDS PAGE.

For Kd determination, F(ab)$_1$POM fragments were generated from the POM antibodies using immobilized papain (10-20 mg of mAb ml^{-1} of immobilized papain as packed resin) activated in digestion buffer (20 mM sodium phosphate, 10 mM EDTA, 20 mM cysteine hydrochloride, pH 7.0) according to the manufacturer's instructions (Pierce, Rockfort, IL). The reaction mixture was incubated overnight with rigorous shaking at 37°C. The digest was separated from the immobilized papain with a resin separator. The immobilized papain was then washed with binding buffer (Protein A IgG Binding Buffer, Pierce) which was added to the digest.

To remove undigested IgG and Fc fragments from the F(ab)$_1$ fragments, the digest was loaded onto a 2 ml Protein A plus Agarose column (Pierce), equilibrated in binding buffer, and washed with 6 ml binding buffer. The F(ab)$_1$-containing flow-through and wash fractions were pooled and further purified by size exclusion chromatography as described above.

Periplasmic expression and purification of scFvPOM1, scFvPOM2, rmPrP$_{23-230}$ and rmPrP$_{90-230}$:

For periplasmic expression and purification of scFv^{POM2}, the pET-22b(+) vector (Novagen) was used, as it has both periplasmic localization and C-term 6xHis tag sequences. The scFvPOM2 gene, constructed previously using the phage display method[3], was inserted into the pET-22b(+) vector between the restriction sites- *Eco*RI and *Xho*I. The resulting plasmid was transformed into competent Rosetta^{TM} (DE3) pLysS cells by heat-shock.

A fresh, single colony of transformed Rosetta cells was inoculated in 2xYT media with 100 µg ml^{-1} Ampicillin and 34 µg ml^{-1} Chloramphenicol (2xYT-AC media) and grown overnight at 37°C at 250 rpm. The overnight culture was further propagated (1:1000) in fresh 2xYT-AC media until the OD_{600} reached ~0.4-0.5. The culture was then cooled down to 25°C in a cold water bath and induced with Isopropyl β-D-1-thiogalactopyranoside (IPTG) to a final concentration of 0.5 mM. The induction was allowed to continue overnight at 25°C and 250 rpm. The cells were harvested and resuspended in 50 ml l^{-1} of the original culture volume of freshly prepared, pre-chilled periplasmic extraction buffer [200mM Tris-HCl, 20% (w/v) sucrose, 1 mM EDTA pH-8.0] and incubated on ice for 1 hour with occasional stirring. The suspension was spun down at 15,000xg for 30 min at 4°C and the supernatant was collected as the soluble protein extract. The extract was thoroughly dialyzed against 50 mM Tris-HCl, 100 mM NaCl, pH 7.0 at 4°C and further clarified by centrifugation at 15,000xg for 30 min at 4°C[40].

The clarified soluble protein extract was loaded onto a Ni-NTA agarose (Qiagen) column equilibrated with 50 mM Tris and 100 mM NaCl, pH 7.0. The unbound protein and impurities were washed off with 50 mM Tris, 100 mM NaCl and 50 mM Imidazole pH 7.0 and the elution

was performed with 50 mM Tris, 100 mM NaCl and 500 mM Imidazole pH 7.0. The purity of the eluates was checked using gel electrophoresis. Pure $scFv^{POM2}$ samples were dialyzed against 50 mM Tris, 100 mM NaCl and 50 mM Imidazole pH 7.0 and concentrated to ~3 mg ml^{-1}. The same procedures applied to expression and purification of periplasmic $scFv^{POM1}$ except the induction was at 17°C. Recombinant mouse PrP was generated in bacteria and purified as reported elsewhere[29,41].

SPR measurements and binding affinity determination

Aminoterminal truncated $rmPrP_{90-230}$ and full-length $rmPrP_{23-230}$ were immobilized on a carboxymethylated-dextran sensor chip (CM5, Biacore) by standard EDC/NHS chemistry. The amount of protein immobilized on the surface corresponded to 1000 Resonance Units (RU) of $rmPrP_{23-230}$ and 4600 RU of $rmPrP_{90-230}$ for comparing $F(ab)_1$POM1 binding in the absence of the OR. For comparing different $F(ab)_1$ affinities, a density of 100 RU of $rmPrP_{23-230}$ was used (Supplementary Table 1). Various concentrations of $F(ab)_1$ measurements were performed on a Biacore T100 at 37°C. $F(ab)_1$ fragments, diluted in running buffer (HBS-EP+), and at a concentration range of 0.01-5.12 nM were injected for 350s at a flow rate of 30 µl min^{-1}. The sensor surface was regenerated between each measurement with 20 mM NaOH. Binding affinity was determined by using the instrument software (Biacore T100 Evaluation Software, version: 2.0.3).

Immunocytochemistry

For immunocytochemistry, organotypic slices were washed twice in PBS and fixed in 4% formalin overnight at 4°C. Membrane inserts were washed and incubated for 1 h in blocking buffer (0.05% vol/vol Triton X-100 and 3% vol/vol goat serum dissolved in PBS) and incubated

with conjugated mouse anti-NeuN-Alexa^{488} (0.5 µg ml^{-1}, Millipore) antibody diluted in blocking buffer at 4°C for 3 d. Inserts were washed four times with PBS and counterstained with 4,6-diamidino-2-phenylindole (dapi) (1 µg ml^{-1}). For NeuN morphometry images were recorded at 4x magnification on a fluorescence microscope (BX-61, Olympus) equipped with a cooled black/white CCD camera at identical exposure times. The area of immunoreactivity was determined by morphometry with image analysis software analySIS vs5.0 using identical greyscale threshold settings for identifying positive pixels.

Mice were euthanized after the last scan (either 5, 24 or 72 hours post injection) and brains fixed in 4% formalin. Cerebella were paraffin embedded and 2µm coronal sections were cut and stained. Hematoxylin and eosin staining and NeuN immunohistochemistry were performed according to standard protocols.

Proteolytic assays

Slices were harvested in pools of 18 slices in PBS, 0.5% DOC, 0.5% NP-40 with 2% β-mercaptoethanol and homogenized by trituration. Homogenates were analyzed immediately for DEVDase activity using caspase 3 fluorometric detection kit (Enzo Life Sciences Caspase-3 Activity Assay kit) and normalized to protein concentration. Slices (pools of 18) were homogenized and processed according to the manufacturer's instructions (Biovision Calpain Activity Assay kit). Calpain activity (Ac-LLY-ase) was measured by detecting cleavage of a specific fluorogenic calpain substrate, Ac-LLY-AFC on a fluorescence plate reader (360-nm excitation filter, 440-nm emission filter) and normalizing to protein amount.

Electron microscopy

Slices were washed in Na-phosphate buffer, fixed in freshly prepared 2% PFA + 2.5% GA in 0.1 M Na-phosphate buffer 0.1 M pH 7.4, postfixed in 1% osmium tetroxide for 1-2 hours, dehydrated through a series of graded ethanols and propylene oxide, embedded in Epon and processed for electron microscopy using standard procedures. Grids were examined and photographed in JEOL JEM 100 CX and JEOL JEM 1011 transmission electron microscopes at 80 kV. Nuclear morphology (as presented in Supplementary Figure 10) was determined by counting 11 fields in IgG-treated COCS at 3, 7, and 10 dpe. For POM1-treated COCS, 10 fields at 3 dpe, 12 fields at 5 and 10 dpe, were analyzed. For assessing necrotic, apoptotic and normal POM1-treated slices at 7 dpe, 15, 16 and 20 fields were counted, respectively.

Viability and ROS assays

For propidium iodide (PI) incorporation, slices were incubated for 30 min with PI (5 µg ml^{-1}) and images were recorded in living tissue using a fluorescent microscope (Axiovert 200) equipped with a cooled CCD camera using a 5x objective and analyzed by morphometry. Lucigenin conversion assay was performed at room temperature as follows: Inserts containing 5-10 slices each were washed in PBS and harvested in Krebs-Ringer solution supplemented with complete mini protease inhibitor cocktail (Roche). Samples were triturated with a 30G syringe, and 50 µl of each sample was mixed with 175 µl assay buffer and 0.25 µl lucigenin (10 mM). Background activity was measured using a chemiluminescence reader. Subsequently, 50 µl NADPH (1 mM) was added to each well and the plate was read again. Background activity was subtracted from the NADPH dependent signal and data (each bar: average of 4 inserts ± s.d.) are presented as relative light unit mg^{-1} total protein.

Erythrocyte complement lysis assay

1 ml tail vein blood was collected from *Prnp*$^{o/o}$ and *Prnp*$^{o/o}$*;tg*a*20*$^{+/+}$ mice in 50 µl, 0.5 M EDTA on ice. Red blood cells (RBCs) were pelleted (2000 RPM for 10 min at RT) and washed in ice-cold PBS thrice. RBCs were resuspended cells in GVB^{2+} buffer (0.15 mM $CaCl_2$, 141 mM NaCl, 0.5 mM $MgCl_2$, 0.1% gelatin, 1.8 mM sodium barbital and 3.1 mM barbituric acid, pH 7.3 and aseptically filtered) and sensitized to complement lysis by incubation with complement activating antibody (34-3C[42], 100 µg ml^{-1} final concentration) or different POM antibodies (100 µg ml^{-1} final concentration) for 1h at RT. RBCs were washed in ice-cold PBS thrice, resuspended in GVB^{2+} buffer and 5 x 10^7 cells were incubated with different concentrations of serum diluted in GVB^{2+} buffer in a total volume of 125 µl. RBCs were incubated for 30 min at 37°C, pelleted by centrifugation and 100 µl supernatant was transferred to a transparent 96 well plate and the absorbance at 414 nm was determined. Relative lytic activity was defined as the serum dilution factor leading to 30% erythrocyte lysis, calculated from the fitted serum dilution curves.

Protein expression and isotopic labelling

For the expression of uniform [^{2}H,^{15}N]-labeled rmPrP$_{23\text{-}230}$, M9 medium was produced from D_2O. M9 medium was supplemented with magnesium chloride, vitamins, ampicillin (final concentration: 100 µg ml^{-1}) and ammonium chloride (2g l^{-1}). The main culture was started by transferring cells from a 2l preculture of LB medium grown to an OD 1.6 at 37°C into 2 liter of M9 D_2O medium. Cells were further incubated for 1h at 37°C and induced by addition of 1 mM IPTG. After 6h cells were harvested and rmPrP$_{23\text{-}230}$ was purified according to our standard protocol[29,43].

NMR experiments

The [^{15}N,^{2}H]- transverse relaxation optimized spectroscopy (TROSY) NMR[44] experiments of the free ^{2}H,^{15}N-labeled rmPrP$_{23\text{-}230}$ and in complex with scFv^{POM1} were performed on a Bruker Avance 700 MHz spectrometer equipped with a 5 mm triple-resonance cryoprobe and a single pulsed field gradient in 10 mM sodium phosphate, pH 7.3, and 5% (v/v) D_2O at 20°C. The data were processed by the software XwinNMR, version 3.5 (Bruker, Germany) and further analysed by the program CARA (www.nmr.ch)[45]. For the assignment of residues 89-230 the assignments deposited in the BioMagResBank (accession numbers: mPrP$_{90–231}$, 16071; numeration according to human PrP) were used, whereas for residues 23-88 a tentative assignment was performed based on the available assignments at pH 4.5[46].

Statistical analysis of COCS

One-way ANOVA with Tukey's post-test for multi-column comparison, or Dunnett's post-test for comparison of all columns to a control column, were used for statistical analysis of experiments involving the comparison of three or more samples. Paired Student's t-test was used for comparing two samples. Results are displayed as the average of replicas ± s.d.

Statistical analysis of MEMRI data sets

For statistical analysis of experiments involving the comparison of three or more data sets, we used one-way ANOVA with Dunnett's post-test for comparison of all data sets to a control data set. One or two-tailed unpaired Student's t-test was used for comparing two data sets. Results are displayed as mean ± s.d. *: P<0.05; **: P<0.01; ***: P<0.001, ****: P<0.0001.

Data collection and structure determination

Diffraction quality POM1 F(ab)$_1$:rmPrP$_{120\text{-}230}$ protein complex crystals were grown by the vapor diffusion method at room temperature as described by Baral et al [47]. X ray diffraction data were measured at the Stanford Synchrotron Radiation Laboratory (SSRL), beamline 9-2[48,49,50]. The data were processed in space group *C2* to a resolution of 1.9Å using the program HKL2000[51]. The data collection details as well as the refinement statistics are presented in Supplementary Table 3. The structure of POM1 F(ab)$_1$:rmPrP$_{120\text{-}230}$ protein complex was solved by the molecular replacement method using the program MOLREP[52] of the CCP4 package [53]. The coordinates of POM1 F(ab)$_1$:huPrP$_{120\text{-}230}$ protein complex, protein data bank (PDB ID: 4DGI), were used as the template. Solution from the molecular replacement was then refined by restrained refinement, implemented in the refinement program of the PHENIX package [54]. The progress of the refinement process was monitored by a reduction in both the R_{work} and R_{free} factors to final values of 19.9% and 23.4%, respectively. Solvent molecules are added to the model by an automated PHENIX program and those water molecules were accepted only when well defined positive peaks were present in both the $2|F_o|-|F_c|$ and $|F_o|-|F_c|$ electron density maps and there was a satisfactory hydrogen-bonding network with either protein atoms or other water molecules. Model building was performed with the program COOT[55]. The final structural coordinates for the POM1 F(ab)$_1$:rmPrP$_{120\text{-}230}$ complex were validated with MOLPROBITY[56] and deposited in the RSCB PDB (accession code 4H88) along with the structure factors. MOLPROBITY showed that 96.8% of the amino acid residues were in the most favored region of the Ramachandran plot. All illustrations were created with the program Pymol (www.pymol.org).

Supplementary references

31 Aller, M. I. *et al.* Cerebellar granule cell Cre recombinase expression. *Genesis* **36**, 97-103, (2003).

32 Mallucci, G. R. *et al.* Post-natal knockout of prion protein alters hippocampal CA1 properties, but does not result in neurodegeneration. *Embo J* **21**, 202-210, (2002).

33 Radovanovic, I. *et al.* Truncated Prion Protein and Doppel Are Myelinotoxic in the Absence of Oligodendrocytic PrPC. *J. Neurosci.* **25**, 4879-4888, (2005).

34 Prinz, M. *et al.* Intrinsic resistance of oligodendrocytes to prion infection. *J Neurosci* **24**, 5974-5981, (2004).

35 Heppner, F. L. *et al.* Experimental autoimmune encephalomyelitis repressed by microglial paralysis. *Nat Med* **11**, 146-152, (2005).

36 Levites, Y. *et al.* Intracranial adeno-associated virus-mediated delivery of anti-pan amyloid beta, amyloid beta40, and amyloid beta42 single-chain variable fragments attenuates plaque pathology in amyloid precursor protein mice. *J Neurosci* **26**, 11923-11928, (2006).

37 Grunecker, B. *et al.* Fractionated manganese injections: effects on MRI contrast enhancement and physiological measures in C57BL/6 mice. *NMR Biomed* **23**, 913-921, (2010).

38 Faas, H. *et al.* Context-dependent perturbation of neural systems in transgenic mice expressing a cytosolic prion protein. *Neuroimage* **49**, 2607-2617, (2010).

39 Falsig, J. *et al.* A versatile prion replication assay in organotypic brain slices. *Nat Neurosci* **11**, 109-117, (2008).

40 Das, D., Allen, T. M. & Suresh, M. R. Comparative evaluation of two purification methods of anti-CD19-c-myc-His6-Cys scFv. *Protein Expr Purif* **39**, 199-208, (2005).

41 Lysek, D. A. & Wüthrich, K. Prion protein interaction with the C-terminal SH3 domain of Grb2 studied using NMR and optical spectroscopy. *Biochemistry* **43**, 10393–10399, (2004).

42 Baudino, L. *et al.* IgM and IgA anti-erythrocyte autoantibodies induce anemia in a mouse model through multivalency-dependent hemagglutination but not through complement activation. *Blood* **109**, 5355-5362, (2007).

43 Hornemann, S., Christen, B., von Schroetter, C., Perez, D. R. & Wuthrich, K. Prion protein library of recombinant constructs for structural biology. *FEBS J* **276**, 2359-2367, (2009).

44 Pervushin, K., Riek, R., Wider, G. & Wuthrich, K. Attenuated T2 relaxation by mutual cancellation of dipole-dipole coupling and chemical shift anisotropy indicates an avenue to NMR structures of very large biological macromolecules in solution. *Proc Natl Acad Sci U S A* **94**, 12366-12371, (1997).

45 keller, R. (ed Goldau Cantina Verlag, Switzerland) (2004).

46 Riek, R. *NMR of the mouse prion protein*, ETH Zürich, Nr. 12759,(1998).

47 Baral, P. K. *et al.* Crystallization and preliminary X-ray diffraction analysis of prion protein bound to the Fab fragment of the POM1 antibody. *Acta Crystallogr Sect F Struct Biol Cryst Commun* **67**, 1211-1213, (2011).

48 Cohen, A. E., Ellis, P. J., Miller, M. D., Deacon, A. M. & Phizackerley, R. P. An automated system to mount cryo-cooled protein crystals on a synchrotron beamline, using compact sample cassettes and a small-scale robot. *Journal of Applied Crystallography* **35**, 720-726, (2002).

49 Gonzalez, A. *et al.* Web-Ice: integrated data collection and analysis for macromolecular crystallography. *Journal of Applied Crystallography* **41**, 176-184, (2008).

50 McPhillips, T. M. *et al.* Blu-Ice and the Distributed Control System: software for data acquisition and instrument control at macromolecular crystallography beamlines. *J Synchrotron Radiat* **9**, 401-406, (2002).
51 Otwinowski, Z. & Minor, W. Processing of X-ray Diffraction Data Collected in Oscillation Mode. *Methods in Enzymology* **276**, 307-326, (1997).
52 Vagin, A. & Teplyakov, A. MOLREP: an Automated Program for Molecular Replacement. *Journal of Applied Crystallography* **30**, 1022-1025, (1997).
53 Winn, M. D. *et al.* Overview of the CCP4 suite and current developments. *Acta Crystallographica Section D* **67**, 235-242, (2011).
54 Echols, N. *et al.* Graphical tools for macromolecular crystallography in PHENIX. *Journal of Applied Crystallography* **45**, 581-586, (2012).
55 Emsley, P. & Cowtan, K. Coot: model-building tools for molecular graphics. *Acta Crystallographica Section D* **60**, 2126-2132, (2004).
56 Chen, V. B. *et al.* MolProbity: all-atom structure validation for macromolecular crystallography. *Acta Crystallographica Section D* **66**, 12-21, (2010).
57 Mander, P. & Brown, G. C. Activation of microglial NADPH oxidase is synergistic with glial iNOS expression in inducing neuronal death: a dual-key mechanism of inflammatory neurodegeneration. *J Neuroinflammation* **2**, 20, (2005).
58 Avshalumov, M. V. & Rice, M. E. NMDA receptor activation mediates hydrogen peroxide-induced pathophysiology in rat hippocampal slices. *J Neurophysiol.* **87**, 2896-2903, (2002).
59 Bano, D. *et al.* Cleavage of the plasma membrane Na+/Ca2+ exchanger in excitotoxicity. *Cell* **120**, 275-285, (2005).
60 Fox, J. E., Austin, C. D., Reynolds, C. C. & Steffen, P. K. Evidence that agonist-induced activation of calpain causes the shedding of procoagulant-containing microvesicles from the membrane of aggregating platelets. *J Biol Chem.* **266**, 13289-13295, (1991).
61 Abramov, A. Y., Scorziello, A. & Duchen, M. R. Three distinct mechanisms generate oxygen free radicals in neurons and contribute to cell death during anoxia and reoxygenation. *J Neurosci.* **27**, 1129-1138, (2007).
62 Avshalumov, M. V., Chen, B. T. & Rice, M. E. Mechanisms underlying H(2)O(2)-mediated inhibition of synaptic transmission in rat hippocampal slices. *Brain Res* **882**, 86-94, (2000).
63 Aarts, M. *et al.* A key role for TRPM7 channels in anoxic neuronal death. *Cell* **115**, 863-877, (2003).
64 Hsiao, Y. H., Chen, P. S., Yeh, S. H., Lin, C. H. & Gean, P. W. N-acetylcysteine prevents beta-amyloid toxicity by a stimulatory effect on p35/cyclin-dependent kinase 5 activity in cultured cortical neurons. *J Neurosci Res.* **86**, 2685-2695, (2008).

Supplementary tables

Supplementary Table 1. Table of abbrevations in alphabetic order.

CC2	Charge cluster 2 (residues 94 – 110)
CGC	Cerebellar granular cells
COCS	Cerebellar organotypic slice culture
dpe	Days post-exposure
F(ab)	Fragment antigen binding
FT	N-proximal Flexible tail of PrP^{C} (residues 23 – 124)
FT / GD ligands	Holoantibodies, monovalent $F(ab)_1$ fragments, divalent $F(ab)_2$ fragments and recombinant single-chain antibodies (scFv) binding to the flexible tail or globular domain
GD	Globular domain of PrP^{C} (residues 124 – 230)
MEMRI	Manganese Enhanced Magnetic Resonance Imaging
NMR	Nuclear Magnetic Resonance
NOX2	NADPH oxidase 2
OR	Octapeptide repeats (residues 50-90)
PI	Propidium iodide
pii	Post intracerebellar injection
POMs	Set of 19 anti PrP monoclonal antibodies (Polymenidou 2008)
Prnp	PrP gene locus
$Prnp^{o/o}$	Mice lacking the *Prnp* gene
PrP, PrP^{C}, PrP^{Sc}	Prion protein, cellular Prion protein, Scrapie-associated Prion protein
$PrP\Delta_{32\text{-}93}$, $PrP\Delta_{94\text{-}110}$	Transgenic mice expressing a truncated PrP version (lacking residues 32-93 and 94-110, respectively)
$rmPrP_{23\text{-}230}$	Full length recombinant mouse PrP (residues 23-230)
ROS	Reactive oxygen species
ScFv	Single-chain variable fragment
tga20	Mice overexpressing PrP^{C}

Supplementary Table 2. Synopsis of the antibodies targeting PrP.

	Domain*	Epitope*		Toxicity[#]	GD protection	Affinity (nM)		
		sequence	location			Holo-Ab	$F(ab)_1$	scFv
POM2	FT	GQPHGGG/SW	57-64, 64-72, 72-80, 80-88	-	+	<0.1*	2.5	20*
POM11	FT	GQPHGGSW	64-72, 72-80	-	+		-	-
POM12	FT	GQPHGGG/SW	57-64, 64-72, 72-80,80-88	-			-	-
POM3	HR	HNQWNK	95-100	+/-	+		-	-
POM1	GD	β1-α1 loop, α1 and α3	[¥]138-147; 204/208/212	+		0.58*	2.5	800
POM4	GD	β1 and α3	121-134 and 218-221	+			-	-
POM5	GD	β2-α2 loop, α2	168-174	-			16	-
POM6	GD	β1-α1 loop, α1 β2-α2 loop, α2	140/145; 158/177; 170/174	-			-	-
POM7	GD	β1-α1 loop, α1 β2-α2 loop, α2	140/145; 158/177; 170/174	-			-	-
POM8	GD	β1-α1 loop, α1 β2-α2 loop, α2	140/145; 170/174	+			-	-
POM9	GD	β1-α1 loop, α1 β2-α2 loop, α2	140/145; 170/174	+			-	-
POM10	GD	β1 and α3	121-134 and 218-221	+			-	
POM13	GD	α1		+/-			-	
POM15	GD	β1-α1 loop, α1	140/145	-			5	
POM17	GD	β1-α1 loop, α1	140/145	+			6.6	
POM19	GD	β1 and α3	121-134 and 218-221	+		0.87*	0.4	

*: data from ref.[3], reproduced here for convenience. The reported epitopes are based on peptide competition and differential binding to PrP^C mutants. For POM1, crystallographic coordinates were used. [¥]: The POM1 epitope was characterized by X-ray analysis (Movie S1) and NMR spectroscopy (Supplementary Fig. 9) and revealed an additional contact site on helix3. [#]: +: toxic; -: nontoxic; +/-: moderately toxic

Supplementary Table 3. Crystallographic analysis of the POM1-PrP complex: data collection and refinement statistics.

	POM1 $F(ab)_1$:rmPrP$_{120230}$
Data collection	
Space group	C2
Cell dimensions	
a, *b*, *c* (Å)	83.4, 107.3, 75.4
α, β, γ (°)	90.0, 95.2, 90.0
Resolution (Å)	50-1.90 (1.97-1.90) *
R_{merge}	0.08 (0.52)
$I/\sigma I$	4.2 (3.9)
Completeness (%)	96.0 (74.1)
Redundancy	4.2 (3.9)
Refinement	
Resolution (Å)	50.0-1.90
No. reflections	49,880
R_{work}/ R_{free}	0.19/0.23
No. atoms	
Protein	4153
Ligand/ion	1
Water	359
B-factors	
Protein	42.2
Ligand/ion	12.8
Water	43.7
R.m.s deviations	
Bond lengths (Å)	0.006
Bond angles (°)	0.956

Number of crystals =1.

*Highest resolution shell is shown in parenthesis.

Supplementary Table 4. Description of the tool compounds used in the study.

Compound	Primary target (according to published data)	Protection against POM1
1400W	Nitric oxide synthase 1 and 2 [57]	no
Ascorbate	ROS scavenging [58]	yes
Calpeptin	Cysteine-proteases: Calpains and cathepsins [59,60]	yes
DPI	NOX inhibitor [61]	n/a
Isoascorbate	ROS scavenging[62]	yes
MnTBAP	Superoxide and H_2O_2 scavenging [63]	yes
N-acetyl-cysteine	ROS scavenging [64]	yes
zVAD-FMK	Broad-spectrum caspase inhibitor [59]	no

n/a: not amenable to assessment due to toxic effects

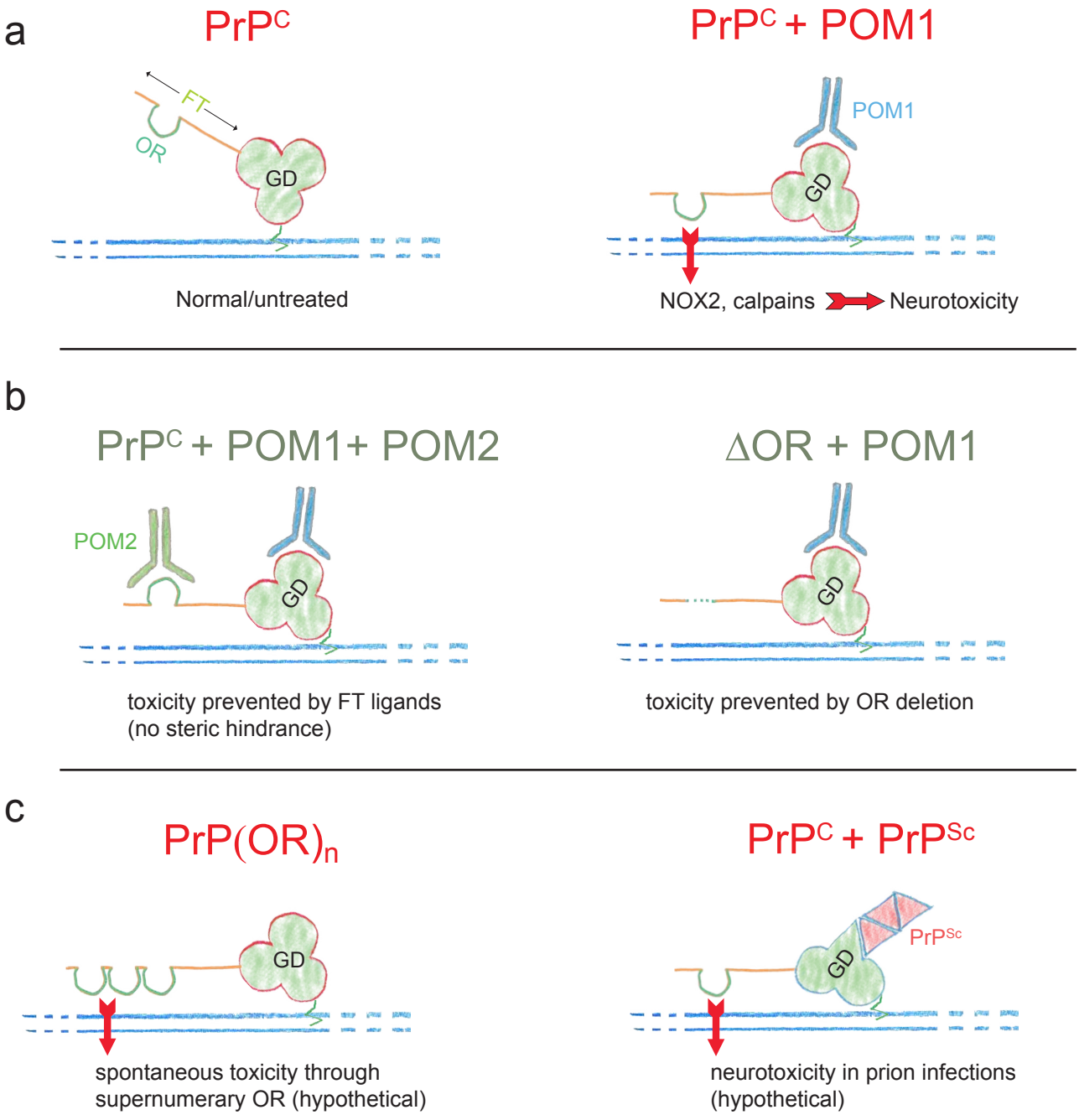

Supplementary Figure 1. Models of PrP-mediated toxicity. a, The cellular prion protein PrP^C consists of a long flexible tail (FT) and a globular domain (GD) tethered to the membrane (blue) via a GPI anchor (green). GD ligands (holoantibodies, F(ab) fragments, or scFv minibodies) trigger neuronal loss, perhaps by altering the conformation of the FT relative to the membrane or to other molecules. **b**, Toxicity was abolished by pretreatment with FT ligands that engaged the octapeptide repeats (OR), or by deleting the OR. **c**, Supernumerary OR are associated with hereditary Creutzfeldt-Jakob disease and may plausibly also exert neurotoxicity through the FT. Bona fide prion infections may also conceivably utilize the same mechanism, as hypothesized in the right panel.

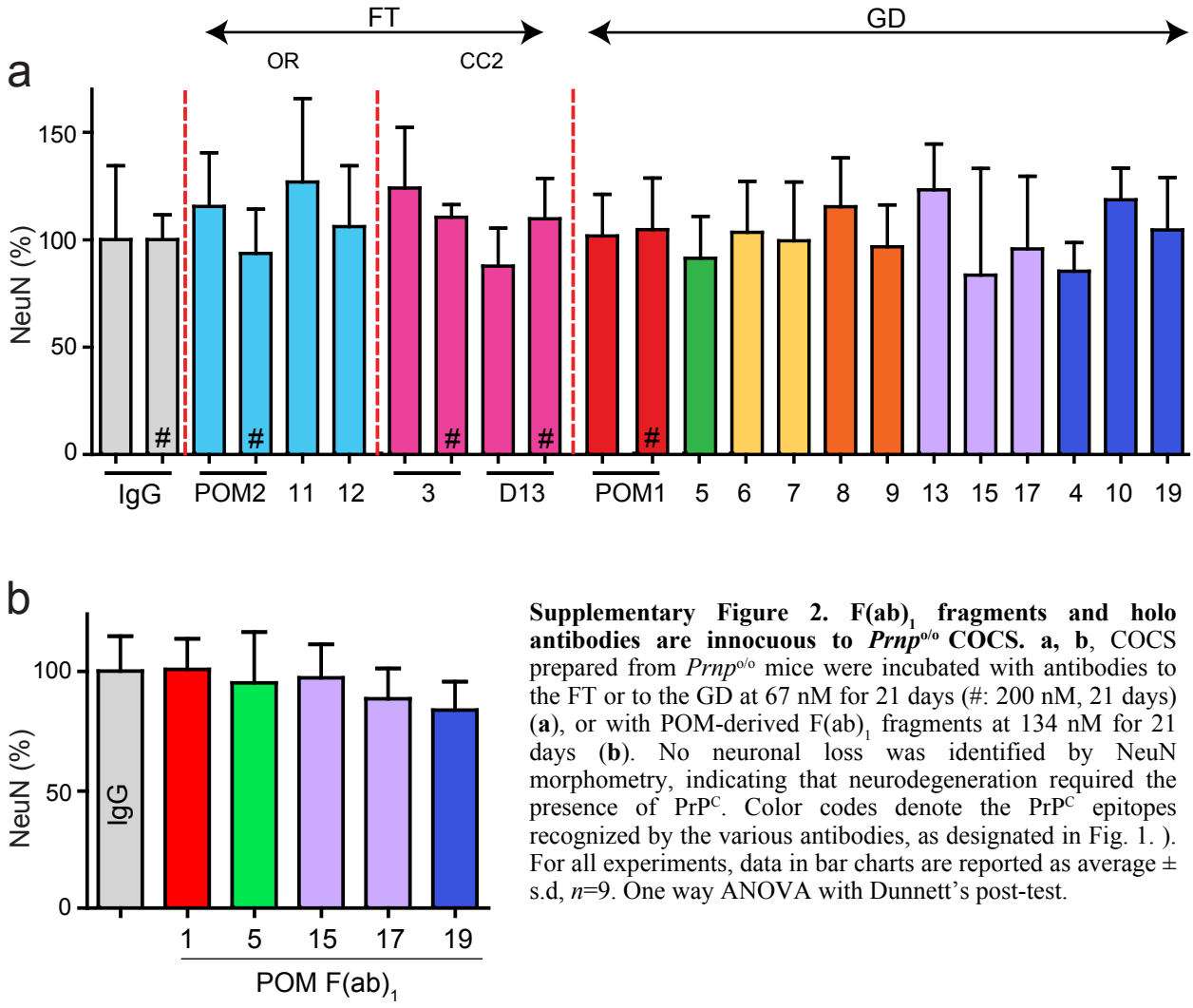

Supplementary Figure 2. F(ab)$_1$ fragments and holo antibodies are innocuous to *Prnp*$^{o/o}$ COCS. a, b, COCS prepared from *Prnp*$^{o/o}$ mice were incubated with antibodies to the FT or to the GD at 67 nM for 21 days (#: 200 nM, 21 days) (**a**), or with POM-derived F(ab)$_1$ fragments at 134 nM for 21 days (**b**). No neuronal loss was identified by NeuN morphometry, indicating that neurodegeneration required the presence of PrP^C. Color codes denote the PrP^C epitopes recognized by the various antibodies, as designated in Fig. 1.). For all experiments, data in bar charts are reported as average ± s.d, *n*=9. One way ANOVA with Dunnett's post-test.

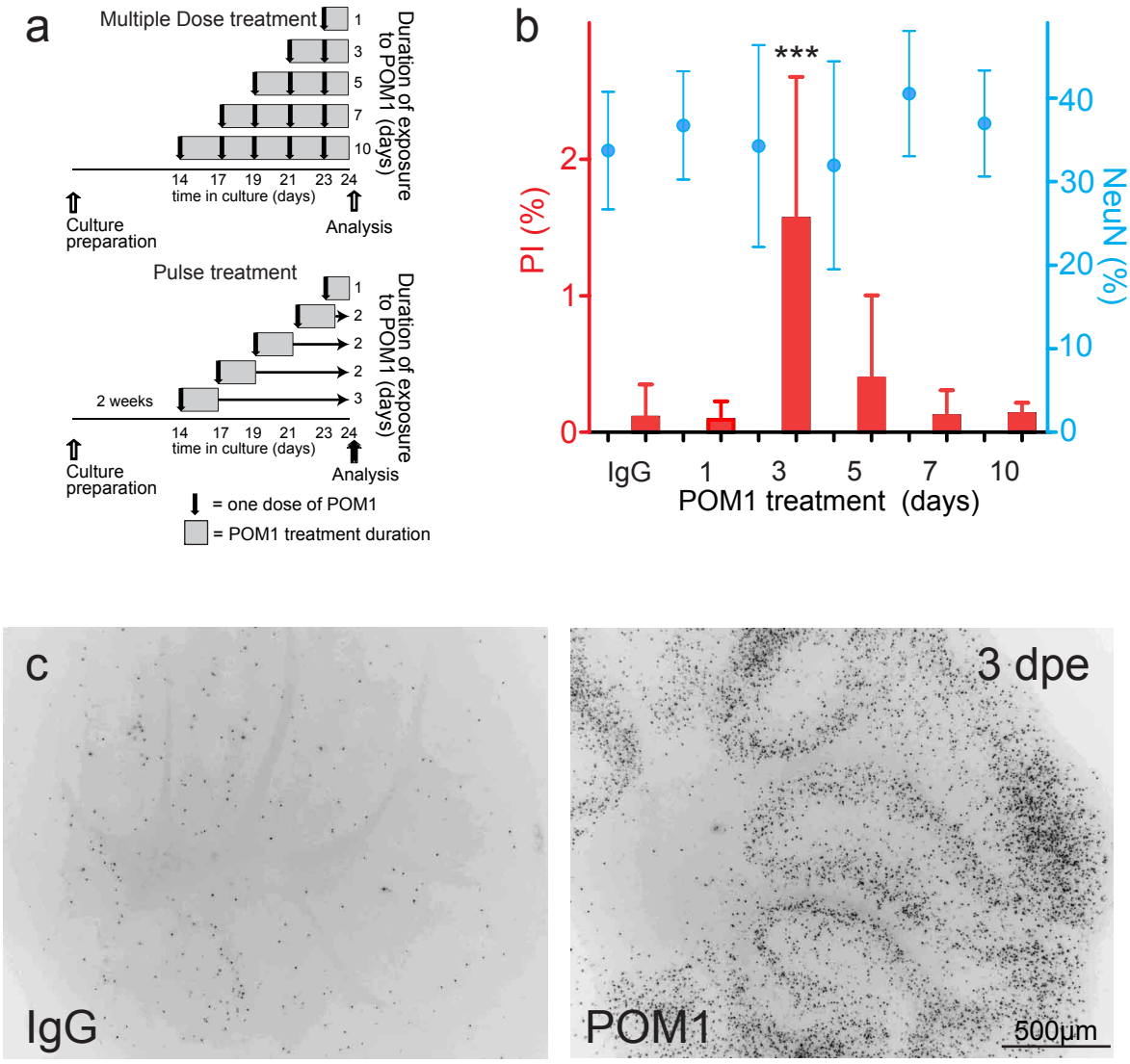

Supplementary Figure 3. COCS viability after pulsed exposure to POM1. a, Treatment scheme for time course analysis. Slices were treated with antibodies either continuously (upper panel) or during pulses as specified (lower panel). **b**, Pulsed treatment. COCS were exposed to POM1 (67 nM) for 24-72h, and subsequently transferred to antibody-free medium. COCS were then cultured for various time intervals, and analyzed by NeuN morphometry (blue) or for PI incorporation (red). Even if short POM1 pulses did not induce histologically conspicuous CGC loss (as seen after protracted treatment), a significant spike of PI incorporation was consistently seen at 3 dpe. Data are reported as average ± s.d, n=9. One way ANOVA with Dunnett's post-test. ***P<0.001. **c**, Conspicuous PI incorporation (dark dots within negative of fluorescent images) in the cerebellar granular layer (CGL) of POM1-exposed *tga20* COCS (3dpe).

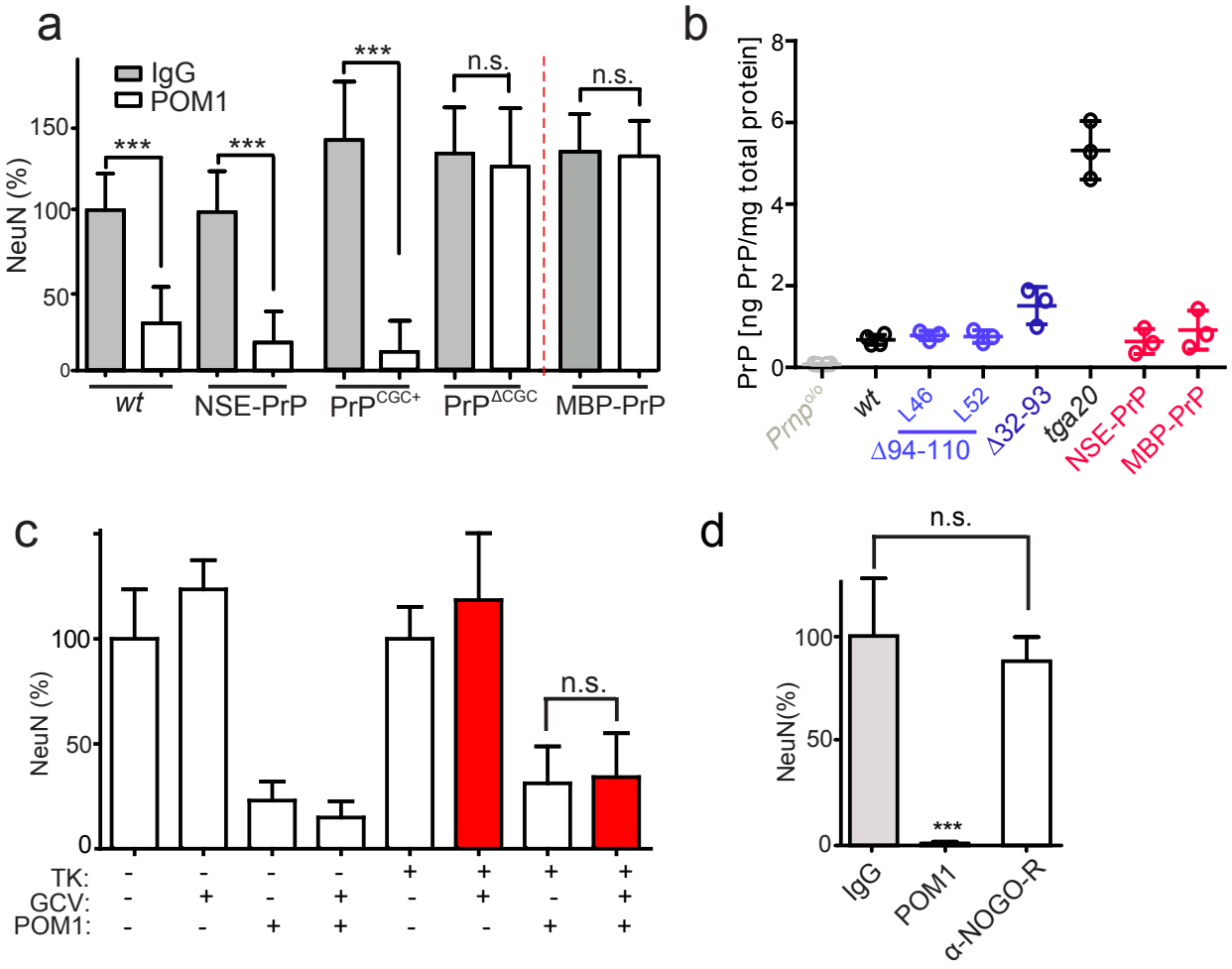

Supplementary Figure 4. Neuronal expression of PrP^{c} is required for antibody-induced neurodegeneration. **a,** POM1 or control pooled IgG (267 nM, 28dpe) were administered to COCS expressing PrP^{C} selectively in neurons (NSE-PrP), to COCS whose CGCs were selectively depleted of PrP^{C} (GABA-A$_{\alpha 6}$-CRE^{+};loxPrP-tg37, termed PrP$^{\Delta CGC}$), to littermate control GABA-A$_{\alpha 6}$-CRE^{-};loxPrP-tg37 (termed PrP^{CGC+}), and to COCS expressing PrP^{C} selectively in oligodendrocytes (MBP-PrP). NSE-PrP and PrP^{CGC+} COCS underwent POM1-induced neurodegeneration, whereas no toxicity was detected in PrP$^{\Delta CGC}$ and MBP-PrP COCS as assessed by NeuN morphometry. One way ANOVA with Tukey's post-test. ***P<0.001, n.s.>0.05. **b**, ELISA assays showing that prion protein expression in the deletion mutants PrP$_{\Delta 94\text{-}110}$ and PrP$_{\Delta 32\text{-}93}$ (violet), as well as in the tissue-specific transgenic mice NSE-PrP and MBP-PrP (red), was similar to that of *wt* mice. Hence the lack of POM1 toxicity in MBP-PrP COCS was not due to low PrP^{C} expression. Data are presented as mean ± s.d., n=3 cerebella, repeated in duplicates. **c**, *Tga20* COCS expressing the Herpes simplex virus thymidine kinase (TK) under the CD11b promoter were treated for 14 days with ganciclovir (GCV), which ablates microglia without affecting neuronal viability[39], and subsequently treated with POM1 (167 nM) for 21 days. NeuN morphometry showed no effect of microglia depletion (red bars) on POM1 toxicity. One way ANOVA with Tukey's post-test. ***P<0.001, n.s.>0.05. **d**, *Tga20* COCS were treated with IgG, POM1 or anti-NOGO-R antibody (67 nM). POM1, but not anti-NOGO-R, induced neurodegeneration, indicating that damage was not a generic consequence of binding GPI-linked proteins. One way ANOVA with Dunnett's post-test. ***P<0.001, n.s.>0.05.). For all experiments, data in bar charts are reported as average ± s.d, n=9.

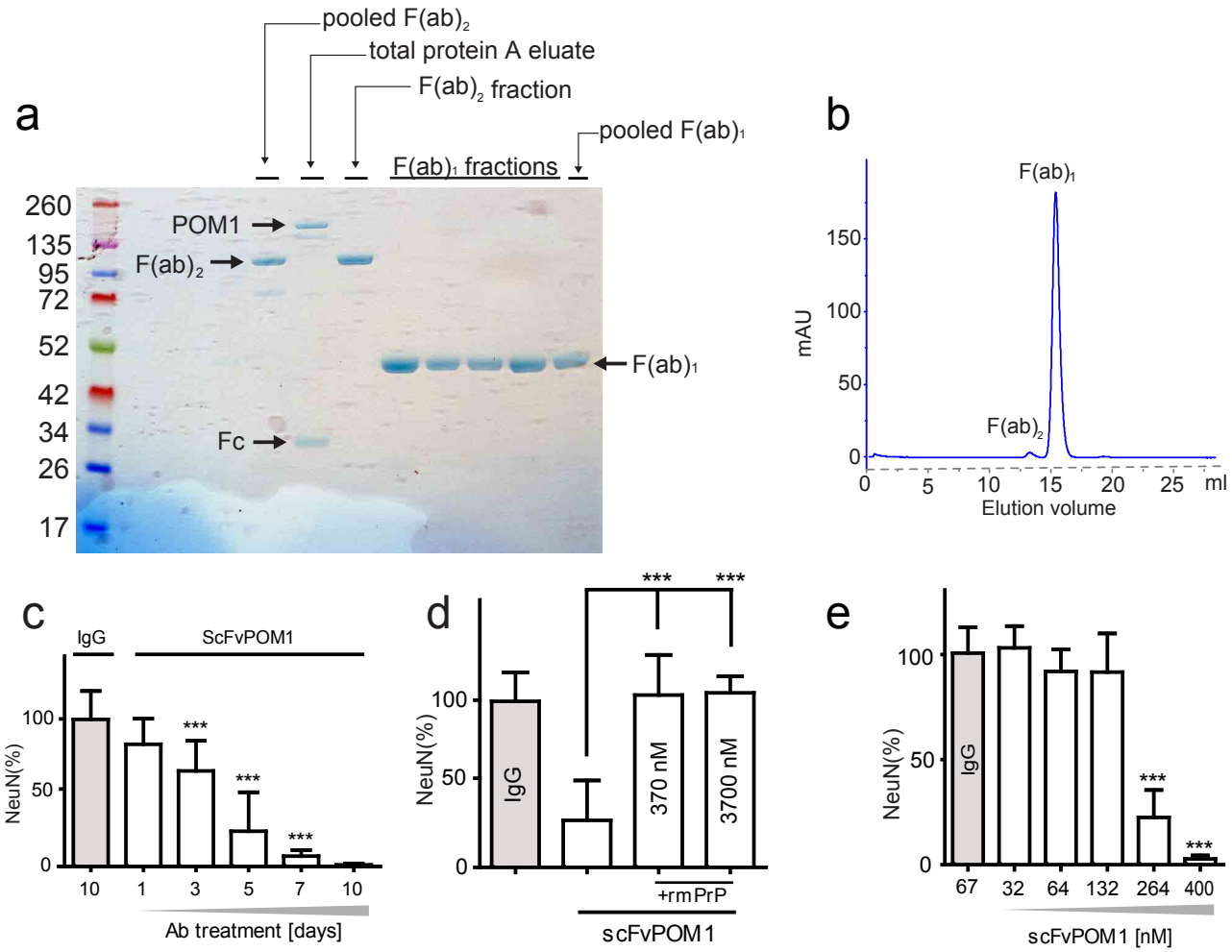

Supplementary Figure 5. Neuronal loss mediated by monovalent antibody fragments. **a**, Purity of antibody preparations, as assessed by Coomassie blue-stained gels. Antibody fragments were obtained through enzymatic digestion of holoantibody and isolated by size-exclusion chromatography. Samples containing either pure $F(ab)_1$ or pure $F(ab)_2$ fragments were pooled and used for experiments. **b**, Pools of $F(ab)_1$ fragments were re-analyzed by size-exclusion chromatography after completion of the COCS exposure experiments. The elution profiles of $F(ab)_1$ fragments confirmed that the $F(ab)_1$ fragment used for experiments did not contain any aggregated $F(ab)_1$. mAU: milliabsorbance units. **c**, Time course of *tga20* slices treated with IgG (67 nM here and henceforth, unless otherwise specified) or $ScFv^{POM1}$ (264 nM). Significant toxicity was present at ≥3 dpe. **d**, *Tga20* slices were treated with IgG, $scFv^{POM1}$ (132 nM), or with $ScFv^{POM1}$ preincubated with $rmPrP_{23\text{-}230}$ (370 or 3700 nM) for 7 days. The presence of $rmPrP_{23\text{-}230}$ blocked the toxicity of scFvPOM1. **e**, *Tga20* slices were exposed to various concentrations of $scFv^{POM1}$ for up to 7 days, and $NeuN^+$ coverage within the CGC layer was assessed morphometrically. Toxicity was conspicuous at 264 nM with kinetics similar to POM1 (Fig. 2f). For all experiments, data in bar charts are reported as average ± s.d, n=9. One way ANOVA with Dunnett's post-test. ***P<0.001.

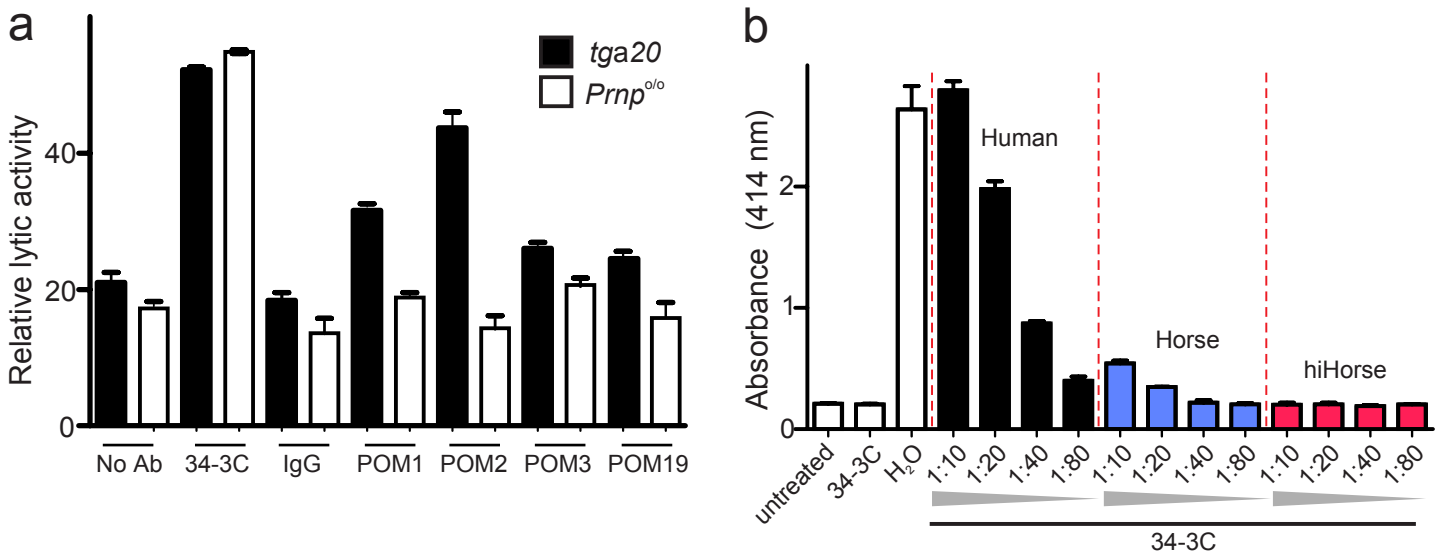

Supplementary Figure 6. Neurotoxicity is independent of complement fixation, and active complement factors are absent from the culture medium. **a**, The relative lytic activities of anti-PrP antibodies[3] (IgG_1) and of the complement-activating antibody 34-3C (positive control, IgG_{2a}) were assessed by pre-incubating *Prnp*$^{o/o}$ (white bars) or *tga20* (black bars) mouse erythrocytes with the respective antibodies. Erythrocytes were then washed and exposed to human serum. Ordinate: dilution of serum mediating 30% lysis of erythrocytes ± s.d., *n*=3. Antibody 34-3C was lytic to both *tga20* and *Prnp*$^{o/o}$ erythrocytes. The highest PrP^C-specific lytic activity was found for POM2, and no lysis was observed with IgG, POM3 or POM19. Hence neurotoxicity does not correlate with complement-mediated lytic activity and is unlikely to be caused by the latter. **b**, *Tga20* erythrocytes were coated with antibody 34-3C, washed, and incubated with various dilutions of normal human serum (black bars), horse serum (blue bars), or heat-inactivated horse serum (hiHorse, red bars). White bars represent erythrocytes left untreated or incubated with 34-3C (negative control) or deionized water (positive control) in the absence of serum. Ordinate: hemoglobin released from lysed erythrocytes was measured spectrophotometrically (Absorbance at 414nm) ± s.d., *n*=4. The complement-fixing antibody 34-3C was highly lytic in human serum, yet failed to lyse erythrocytes in the medium used for culturing COCS, indicating that active complement factors were absent from the culture medium.

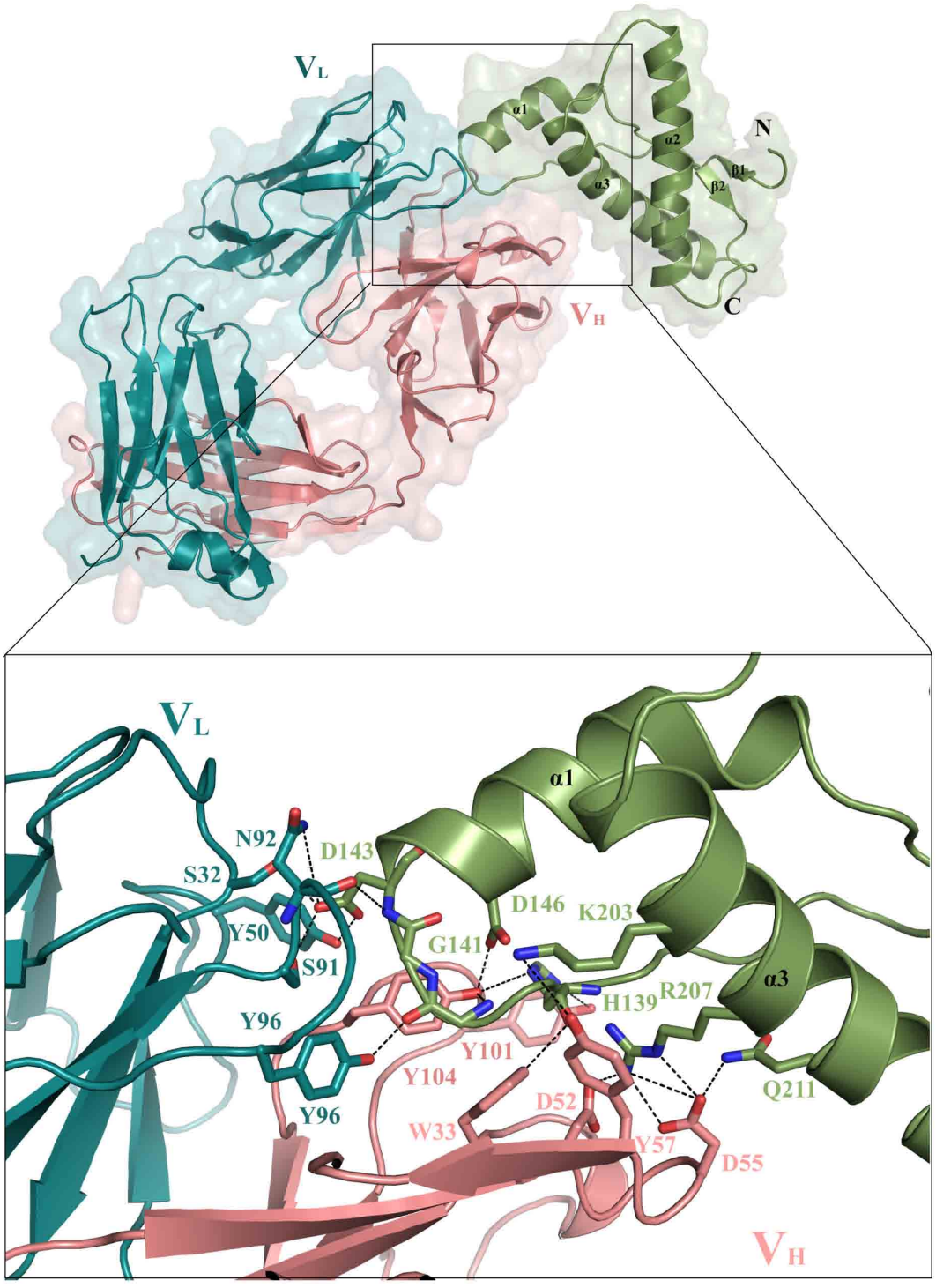

Supplementary Figure 7. X-ray analysis of the complex rmPrP$_{120\text{-}230}$ and F(ab)$_1$POM1. Secondary structure and surface representation of the protein complex between the GD of rmPrP$_{120\text{-}230}$ and F(ab)$_1$POM1. The heavy chain and the light chain of F(ab)$_1$POM1 are represented in salmon and cyan, respectively, whereas rmPrP$_{120\text{-}230}$ is shown in green. A close-up view of the intermolecular contacts between F(ab)$_1$POM1 and rmPrP$_{120\text{-}230}$ is presented below. Interacting residues are displayed in stick representation and hydrogen bonding interactions are shown in black dashed lines.

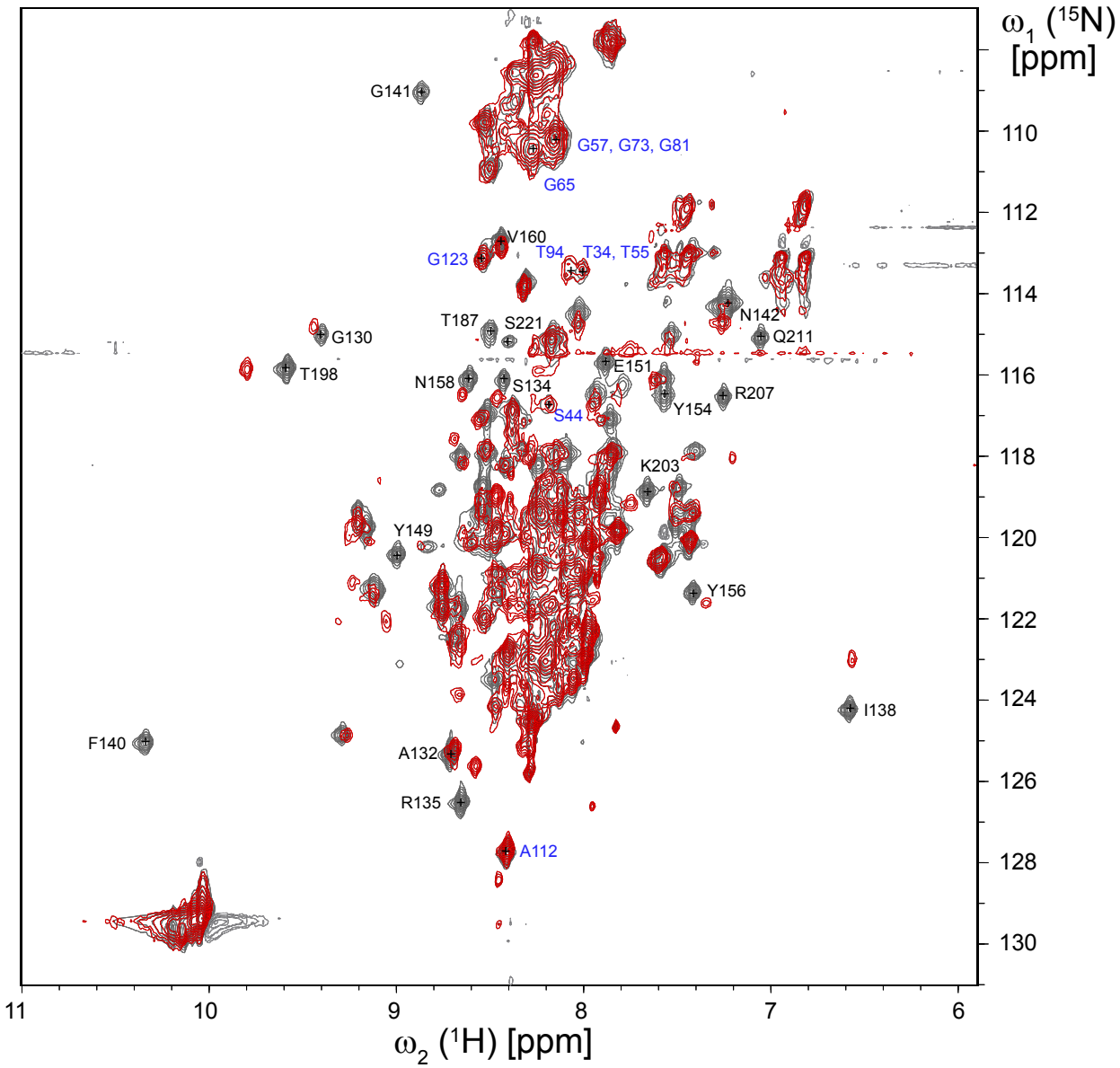

Supplementary Figure 8. NMR analysis of scFv^{POM1} binding to rmPrP$_{23-230}$. Superposition of 2D [^{1}H-^{15}N]-transverse relaxation optimized spectroscopy (TROSY)-spectra of [^{2}H,^{15}N]-labeled rmPrP$_{23-230}$ in the absence (grey spectrum) and presence (red spectrum) of stoichiometric amounts of unlabeled scFv^{POM1}. For simplicity, only isolated cross peaks are marked. Black labels represent residues of rmPrP$_{23-230}$ that are in direct or close contact with scFv^{POM1}. Blue labels indicate the FT. The overlay of the spectra shows the close resemblance of cross peaks to the residues of the FT, indicating that the scFv^{POM1} does not significantly affect the structure of the FT. As expected, strong chemical shift perturbations are observed for residues that directly interact or in close contact with scFv^{POM1}. Minor chemical shift perturbations are also visible for some β1/β2 residues (e.g. G130 and V160).

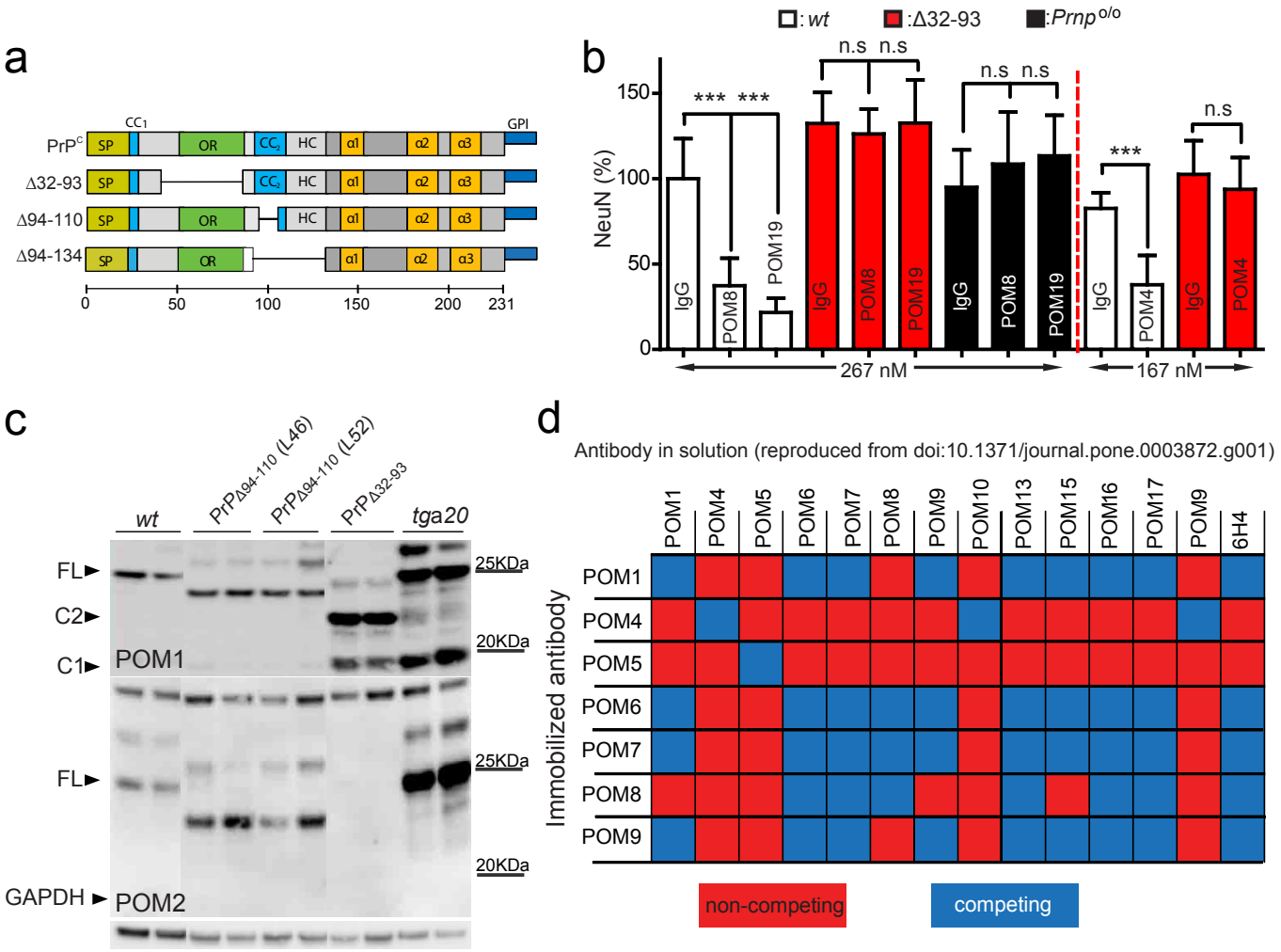

Supplementary Figure 9. The FT transduces GD ligand toxicity. a, Domains of PrP^C and deletion mutants used in Figure 3a, Figure 4e and Figure 4f. SP, signal peptide; OR, Octapeptide repeats; CC1-CC2, charged cluster 1 and 2; HC, hydrophobic core; α1-3, αhelices 1-3; GPI, glycosyl phosphatidyl inositol anchor. **b**, NeuN morphometry of COCS treated with various POM antibodies (167-267 nM, 28 dpe). *Wt* COCS (white) experienced toxicity after exposure to POM4, POM8, or POM19, whereas $PrP_{\Delta 32\text{-}93}$ (red) and $Prnp^{o/o}$ COCS (black) were resistant to the same antibodies. Data are reported as average ± s.d, n=9. One way ANOVA with Tukey's post-test. ***P<0.001, n.s.>0.05. **c**, PrP^C expression levels. PNGase-treated cerebellar homogenates of 10 day-old mice were probed with antibodies to the GD (POM1) and the FT (POM2). While *tga20* pups expressed the highest levels of PrP^C, $PrP_{\Delta 94\text{-}110}$ and $PrP_{\Delta 32\text{-}93}$ pups expressed PrP at levels similar to, or higher than, wild type (*wt*). FL; full-length PrP; C1 and C2: carboxy proximal PrP cleavage fragments (111-230 and 93-230, respectively). As expected, POM2 did not recognize $PrP_{\Delta 32\text{-}93}$ as well as the C1 and C2 cleavage fragments, since it is directed to the octapeptide repeats. **d**, matrix indicating which antibody pairs exhibit competition or steric hindrance (blue) based on SPR competition experiments published elsewhere[3]. These results are reproduced here for convenience and demonstrate that POM1 does not compete with POM5 for a common binding site. **e**, *Tga20* COCS were treated with POM1 (67 nM) in presence or absence of another GD antibody, POM5 (67 nM) for 10 days. POM5 was not toxic by itself, and yet – in contrast to the antibodies directed against the FT – it did not prevent POM1 toxicity. Data are reported as average ± s.d, n=9. One way ANOVA with Dunnett's post-test, n.s.>0.05.

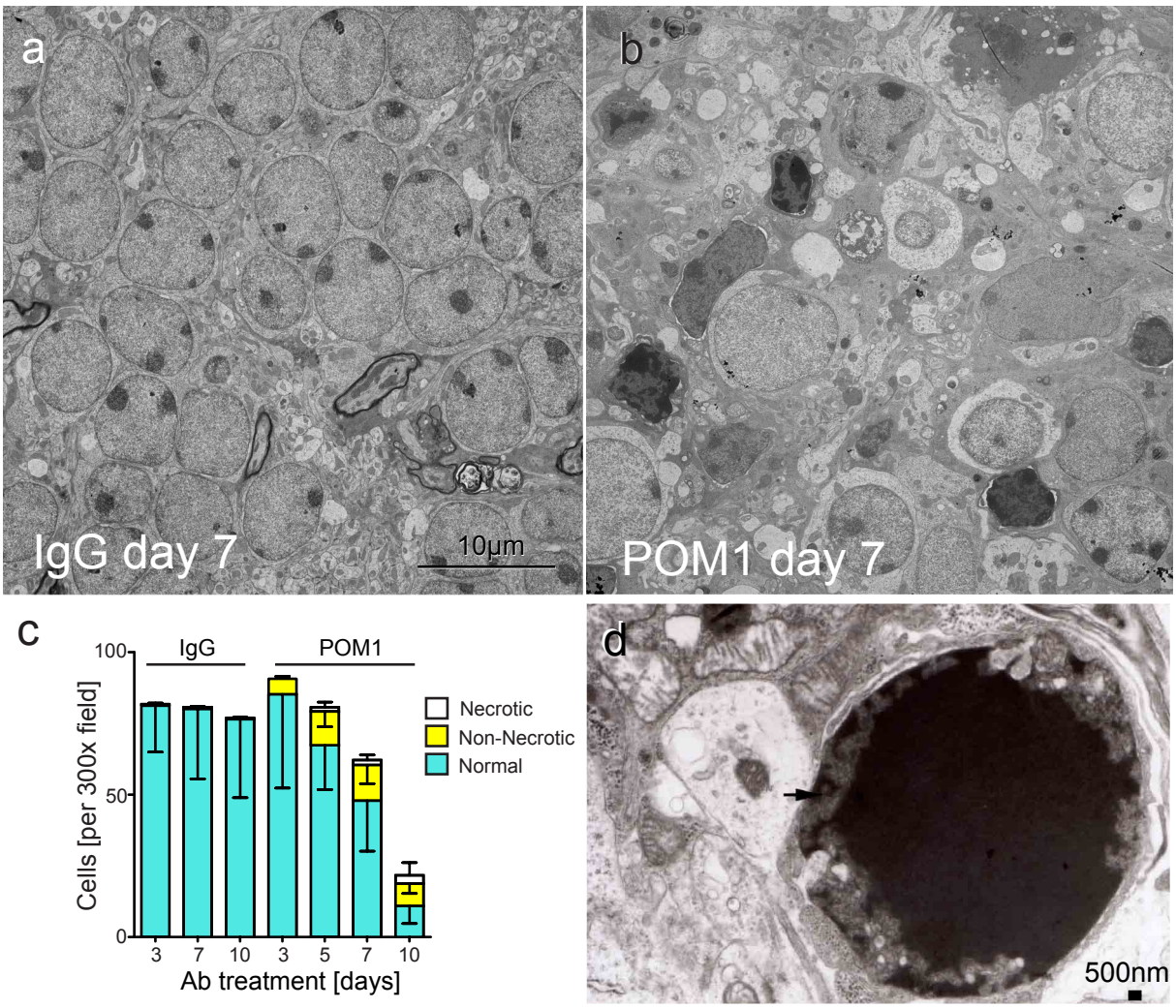

Supplementary Figure 10. Ultrastructural characterization of toxicity in COCS treated with IgG or POM1 (67 nM). a-b, After 7 days of IgG treatment, COCS exhibited healthy CGL morphology (**a)** (magnification: see scale bar), whereas after POM1 treatment, most of CGCs showed irregular and condensed nuclear chromatin (**b**). **c**, Number of cells displaying normal, apoptotic, or necrotic nuclear morphology (average cells/field at x300 magnification ± s.d., at least 10 fields were analyzed) after treatment with POM1 or control IgG for various time periods (3-10 days). **d**, POM1-treated slices at 7 dpe showed nuclear chromatin condensation.

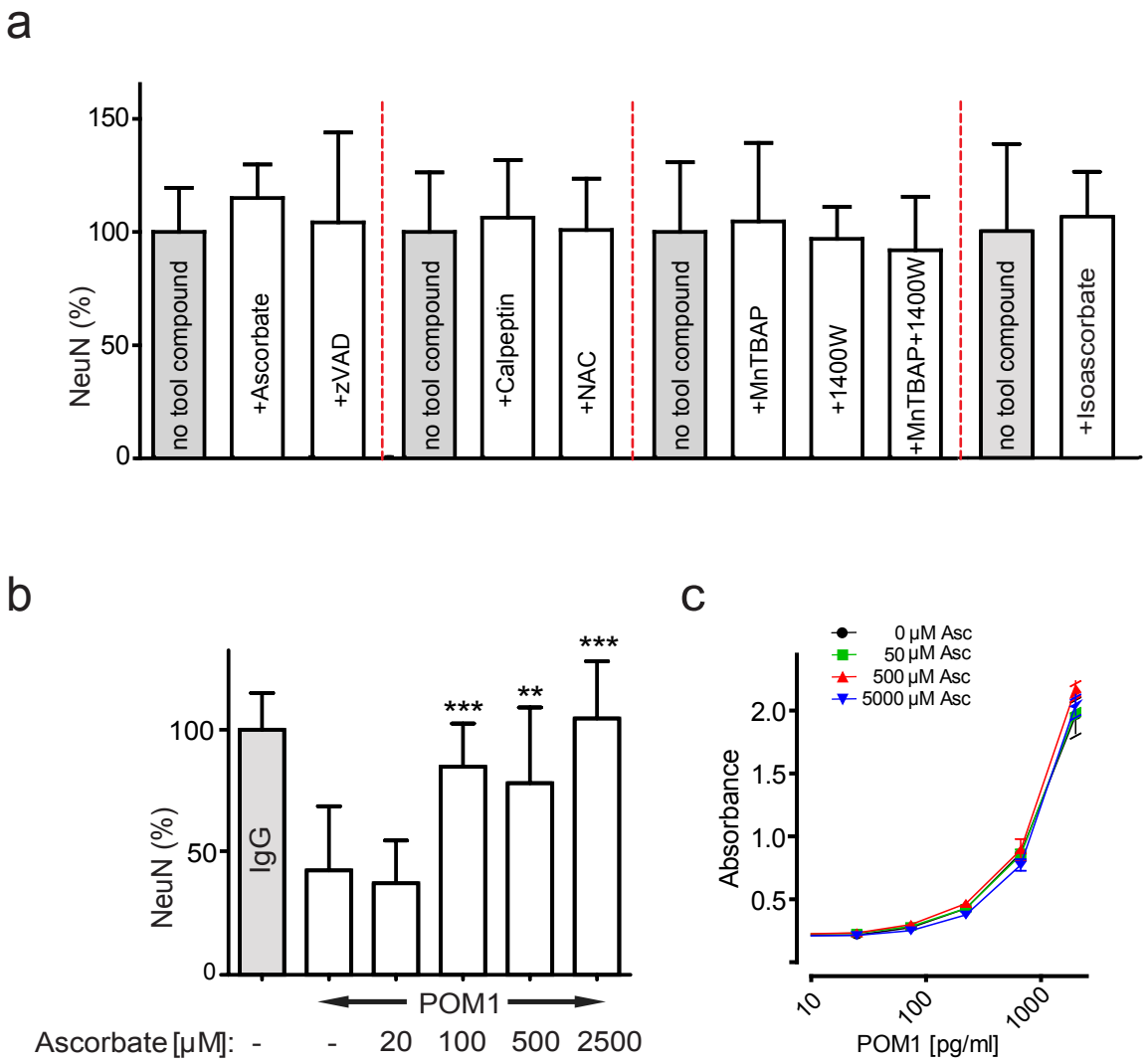

Supplementary Figure 11. Treatment with various tool compounds did not affect viability and antibody binding properties. a, COCS prepared from *tga20* mice were treated with pooled IgG at 67 nM for 10-14 days in the presence of the compounds listed in the figure. Dotted lines delimit biologically distinct experiments, performed on different sets of COCS along with controls. None of the compounds tested affected the viability of COCS, as assessed by NeuN morphometry. **b**, COCS prepared from *tga20* mice were treated with various concentrations of ascorbate and exposed to POM1 (67 nM) for 10 days. Ascorbate was protective at concentrations of >100 µM, but not at 20 µM. For all experiments data in bar charts are reported as average ± s.d, *n*=9. One way ANOVA with Dunnett's post-test. ***P<0.001, **P<0.01. **c**, Aliquots of POM1 were incubated with various concentrations of ascorbate (0-5000 µM) for 48h at 37 °C, and subsequently used for detecting $rmPrP_{23-230}$ immobilized on microtiter plates. POM1 was visualized with HRP-conjugated anti-mouse IgG antibody and chemiluminescence. The presence of ascorbate did not exert any influence on the binding capacity of POM1. Each data point represents mean ± s.d, *n*=3.

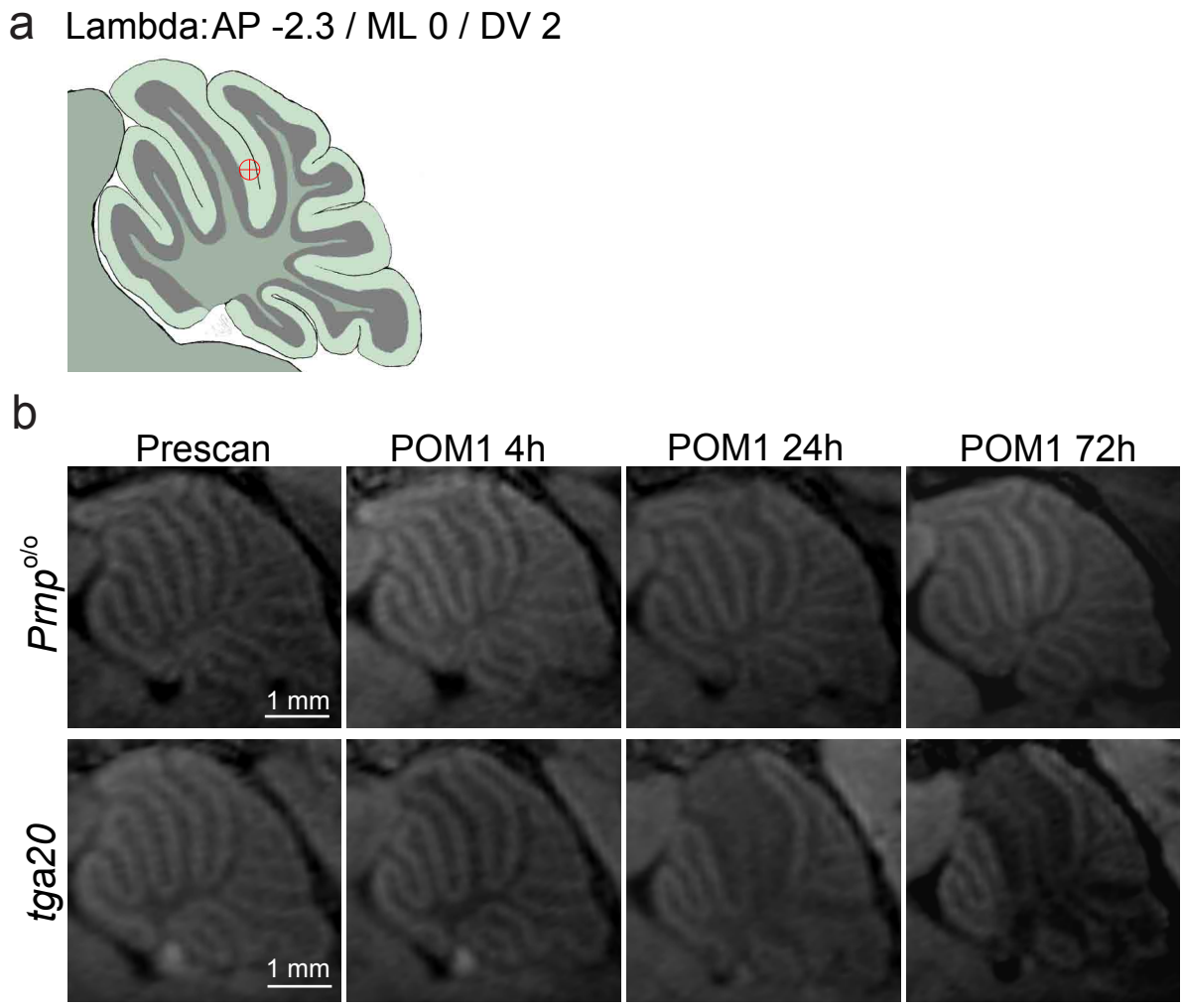

Supplementary Figure 12. Temporal evolution of lesions in mouse cerebella injected with POM1. a, Schematic representation of the murine cerebellum. Crosshairs (red) denote the site of injection. **b**, Representative MRI scans before injection (prescan) and at 4h, 24h, and 72h after POM1 injection in *tga20* and *Prnp*$^{o/o}$ mice. In *tga20* mice, incipient edema was recognizable as marginal hypointensity already at 4h. After 24h and 72h, hypointense lesions were fully developed and involved several folia. In contrast, POM1 injected *Prnp*$^{o/o}$ mice showed only a small hypointensity in the area of the needle tract.

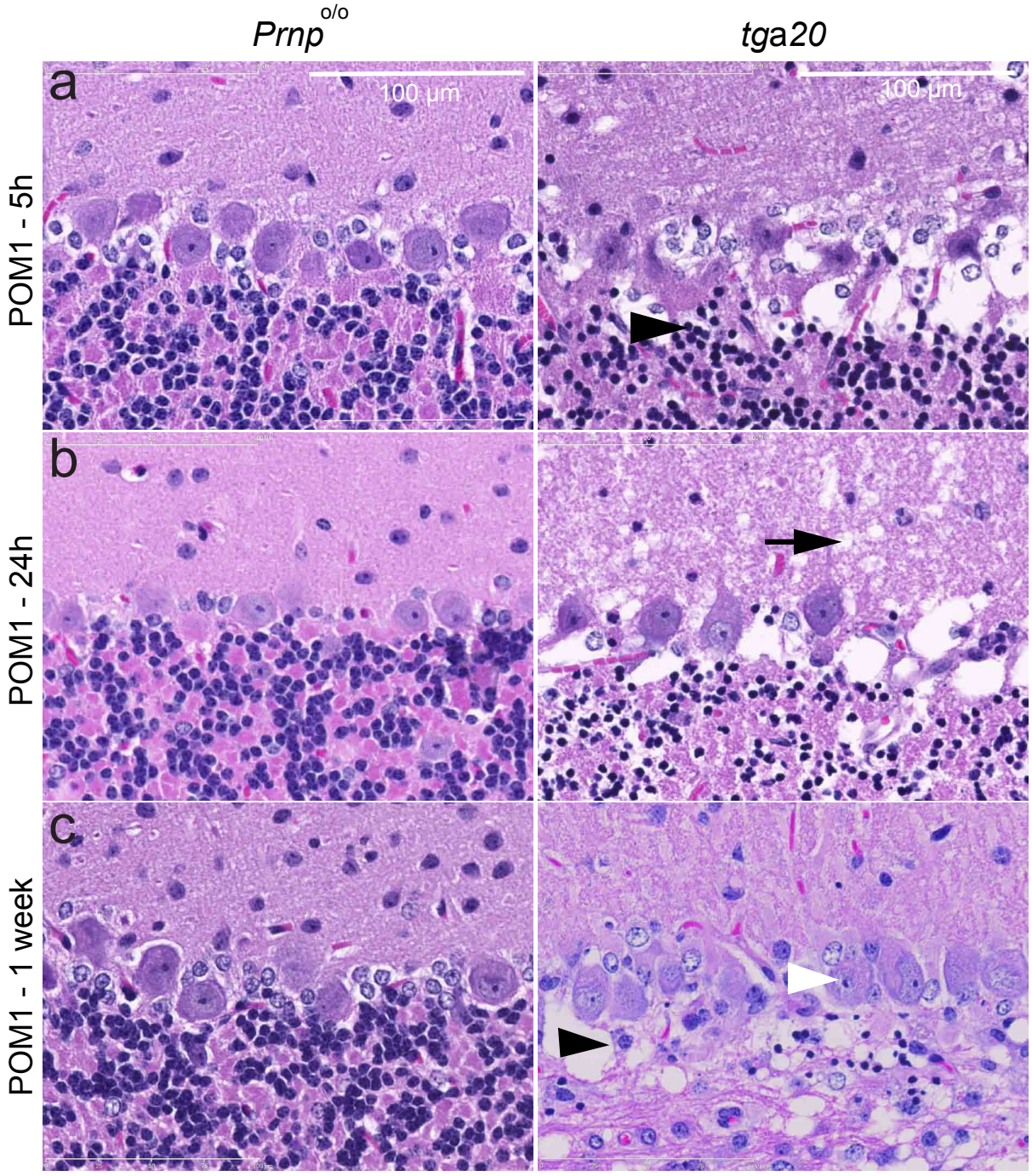

Supplementary Figure 13. Representative hematoxylin-eosin sections from POM1-injected *tga20* and *Prnp*$^{o/o}$ mouse cerebella. a, Chromatin condensation in cerebellar granular cells (black arrow head) was seen as early as 5h post-injection. **b**, Progression to edema and macrophage infiltration (black arrow) was seen after 24h. **c**, One week post injection, prominent loss of granular cell neurons and brisk Bergman glia proliferation (black arrow) were evident. The differential survival of Purkinje neurons (white arrowheads) is consistent with the lack of PrP^C expression in Purkinje neurons of *tga20* mice.

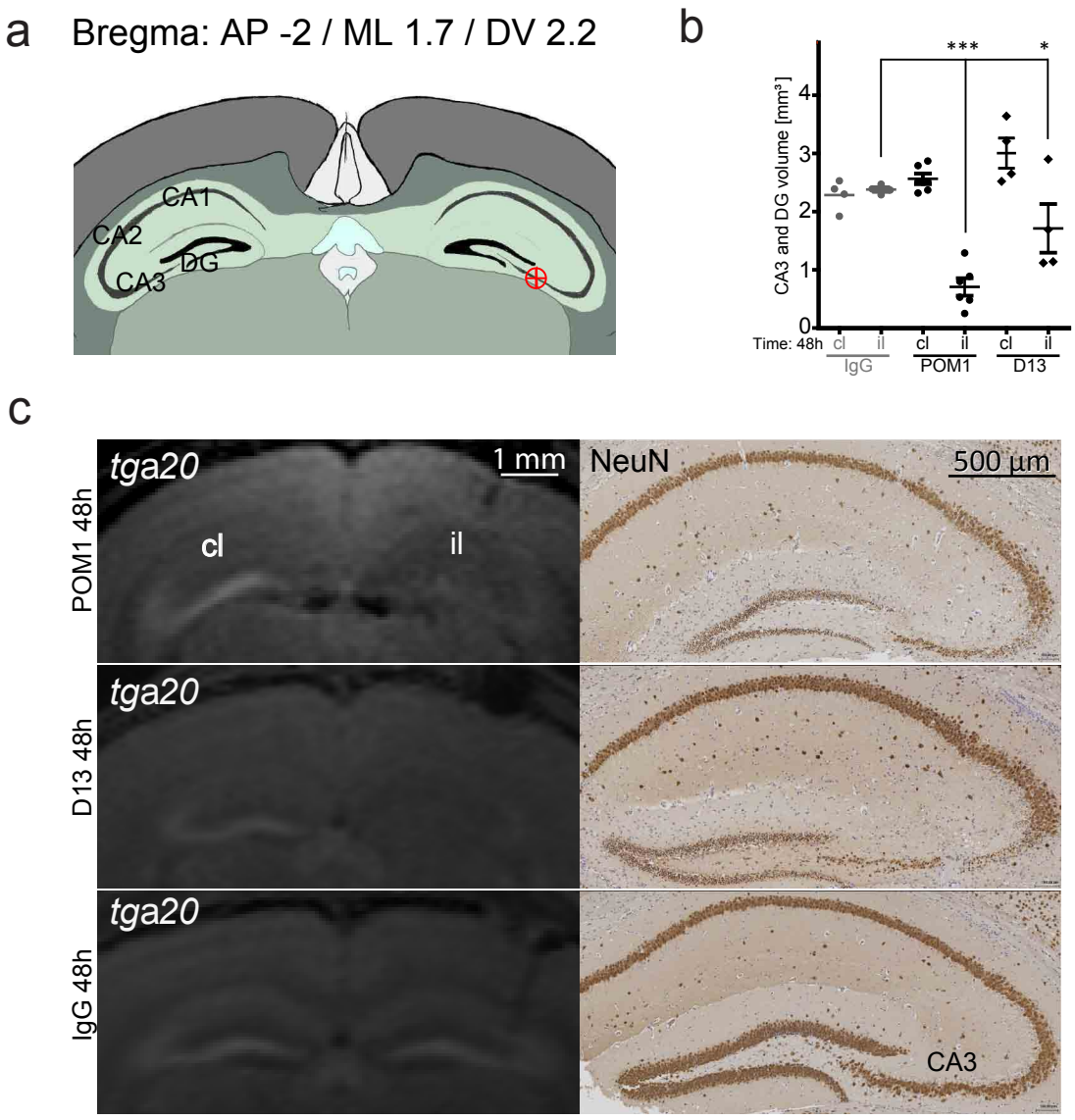

Supplementary Figure 14. Stereotactic injection of POM1, D13 and IgG (6ug) into *tga20* hippocampi. **a**, Schematic representation of the murine hippocampus. Crosshairs (red) denote the site of injection. CA1-3: Cornu ammonis sectors 1-3. DG: Dentate gyrus. **b**, Volumetric assessment of the size of CA3 and DG [mm^3] ipsilaterally (il) and contralaterally (cl) to antibody injection in *tga20* mice (48h post-injection). Both POM1 and D13 led to a reduction in CA3 volume ipsilaterally. Data are presented as mean ± s.d., n=4, One-way ANOVA with Dunnett's post-test, ***P<0.001, *P<0.1.). **c**, MEMRI (left panels) showing loss of the CA2-3 contour and appearance of a hypointense lesion ipsilaterally (il) to the site of POM1 and D13 injection, whereas the contralateral site (cl) did not show lesions after IgG injection. Histological analysis 48h post injection (right panels) showed loss of $NeuN^+$ neurons in the dentate gyrus and in the CA3 sector after POM1 and D13 injection.

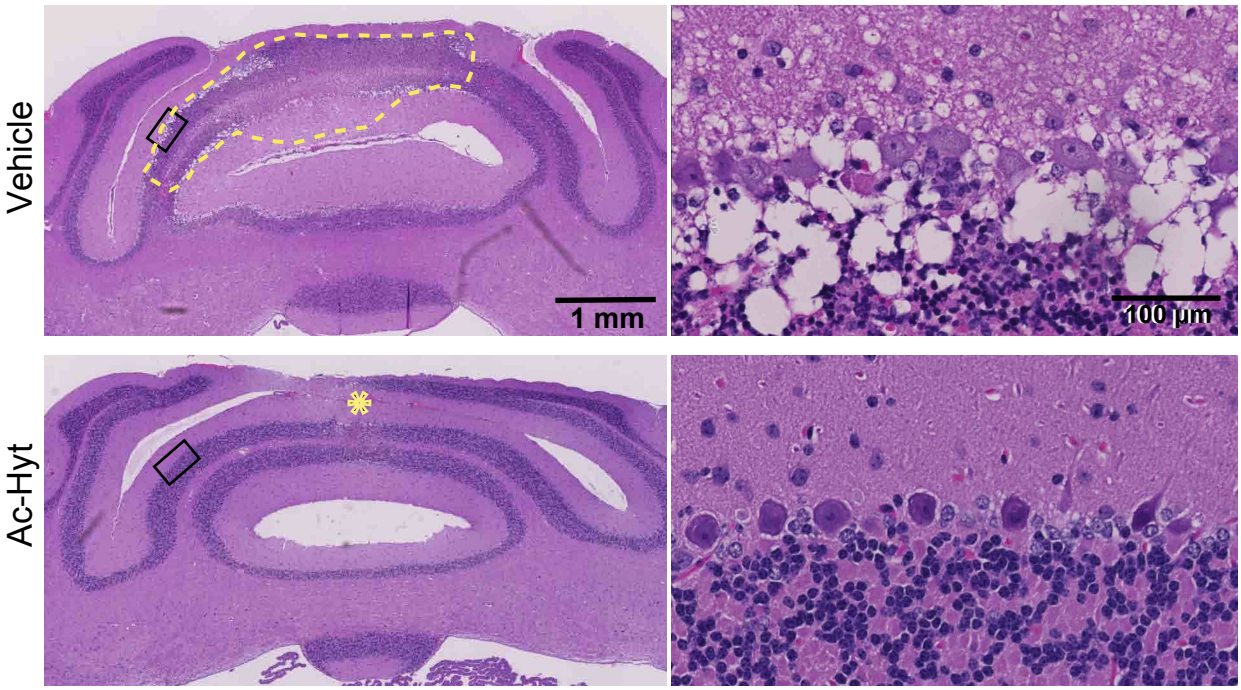

Supplementary Figure 15. a, b, Representative H&E histology of mice pretreated with acetylated hydroxyl tyrosol and injected with scFv^{POM1}. Hematoxylin-eosin stained sections of mouse cerebella. Whereas vehicle-treated mice developed large areas of cell death around the site of injection (yellow dashed line), only small lesions were visible in treated mice in the immediate vicinity of the needle tract (yellow asterisk). Rectangles indicate the position of the high magnification pictures shown in the right-side panels.